Transportation Research Part E 181 (2024) 103367

Contents lists available at ScienceDirect

Transportation Research Part E

journal homepage: www.elsevier.com/locate/tre

Deep bi-directional information-empowered ship trajectory prediction for maritime autonomous surface ships

Huanhuan Li [a,1], Wenbin Xing [b,1], Hang Jiao [c], Zaili Yang [a,*], Yan Li [d]

[a] Liverpool Logistics, Offshore and Marine (LOOM) Research Institute, Liverpool John Moores University, Liverpool, UK
[b] School of Intelligent Systems Engineering, Sun Yat-sen University, Guangdong, China
[c] School of Electronic Information and Communications, Huazhong University of Science and Technology, Wuhan, China
[d] State Key Laboratory of Information Engineering in Surveying, Mapping and Remote Sensing, Wuhan University, Wuhan, China

ARTICLE INFO

Keywords:
AIS data
Ship trajectory prediction
Maritime Autonomous Surface Ships (MASS)
Integrated networks
Maritime safety

ABSTRACT

It is critical to have accurate ship trajectory prediction for collision avoidance and intelligent traffic management of manned ships and emerging Maritime Autonomous Surface Ships (MASS). Deep learning methods for accurate prediction based on AIS data have emerged as a contemporary maritime transportation research focus. However, concerns about its accuracy and computational efficiency widely exist across both academic and industrial sectors, necessitating the discovery of new solutions. This paper aims to develop a new prediction approach called Deep Bi-Directional Information-Empowered (DBDIE) by utilising integrated multiple networks and an attention mechanism to address the above issues. The new DBDIE model extracts valuable features by fusing the Bi-directional Long Short-Term Memory (Bi-LSTM) and the Bi-directional Gated Recurrent Unit (Bi-GRU) neural networks. Additionally, the weights of the two bi-directional units are optimised using an attention mechanism, and the final prediction results are obtained through a weight self-adjustment mechanism. The effectiveness of the proposed model is verified through comprehensive comparisons with state-of-the-art deep learning methods, including Recurrent Neural Network (RNN), Long Short-Term Memory (LSTM), Gated Recurrent Unit (GRU), Bi-LSTM, Bi-GRU, Sequence to Sequence (Seq2Seq), and Transformer neural networks. The experimental results demonstrate that the new DBDIE model achieves the most satisfactory prediction outcomes than all other classical methods, providing a new solution to improving the accuracy and effectiveness of predicting ship trajectories, which becomes increasingly important in the era of the safe navigation of mixed manned ships and MASS. As a result, the findings can aid the development and implementation of proactive preventive measures to avoid collisions, enhance maritime traffic management efficiency, and ensure maritime safety.

1. Introduction

As economic globalisation accelerates, shipping has emerged as a critical mode of transport for facilitating economic exchanges between countries and across regions (Fratila et al., 2021; Li and Yang, 2023; Yang et al., 2021). It benefits from extensive coverage,

* Corresponding author.
E-mail address: Z.Yang@ljmu.ac.uk (Z. Yang).
[1] Equal contribution.

https://doi.org/10.1016/j.tre.2023.103367
Received 17 March 2023; Received in revised form 21 August 2023; Accepted 18 November 2023
Available online 6 December 2023

high transport capacity, and low channel investment. However, complex sea traffic also increases the load on the waterways and port waters, leading to congested traffic flow, heavy management burden, and even collision accidents (Coraddu et al., 2020; Filom et al., 2022; Li et al., 2023b; Luo and Shin, 2019; Ramos et al., 2019; Xin et al., 2023b). The mentioned issues can endanger lives and severely harm the economy. Consequently, it is crucial to accurately perceive and predict ship navigation dynamics, especially regarding ship trajectories.

Maritime Autonomous Surface Ships (MASS), defined by the International Maritime Organization (IMO) as "ships which, to a varying degree, can operate independently of human interaction", are attracting increasing attention in the maritime industry (Chang et al., 2021; Wang et al., 2019). As an emerging area in the current shipping digitalisation, it has bright and broad prospects from all walks of life and will be an important mode of future maritime transportation (Bai et al., 2021; Liu et al., 2022; Veitch and Alsos, 2022). Meantime, extensive exploration and research on the technological development of MASS and its impact on safety and economic areas have been conducted by many scholars (e.g. Chen et al., 2018; Goerlandt, 2020). Trajectory prediction can effectively assist ships in coordinating movements (Kisialiou et al., 2018; Volkova et al., 2021; Zhang et al., 2020), warning against risks (Park et al., 2021), preventing collisions (Alizadeh et al., 2021), and guaranteeing navigation safety (Alessandrini et al., 2019; Statheros et al., 2008).

The Automatic Identification System (AIS) is a comprehensive digital navigation equipment, comprising shore-based (base station) facilities and shipboard equipment (Xin et al., 2023a; Xing et al., 2023; Yin et al., 2022; Zhang et al., 2020). It can combine the Global Positioning System (GPS) to broadcast static and dynamic ship data over Very High Frequency (VHF). This data encompasses Maritime Mobile Service Identity (MMSI), Speed Over Ground (SOG), Course Over Ground (COG), and real-time ship position (longitude and latitude) (Harati-Mokhtari et al., 2007; Li et al., 2017). In December 2000, the IMO officially issued a proposal for the mandatory installation of AIS equipment on ships built after 2002 and on ships operating from 2008 onwards (Yang et al., 2019). Following the explosive of AIS data, maritime and civilian shipping authorities and data centres have accumulated vast AIS history records (Li et al., 2023a; Pallotta et al., 2013; Yan et al., 2022; Zhang et al., 2018). Therefore, the utilisation of AIS data to promote intelligent ship navigation has emerged as a crucial research area (Liang et al., 2022; Sanchez-Gonzalez et al., 2019; Xiao et al., 2022).

Within the context of using AIS data to aid shipping, the methods based on physical or mathematical models require applying kinematic equations under ideal conditions (Sutulo et al., 2002; Tu et al., 2018) and the consideration of multiple influential factors (e.g. mass, yaw angle, and speed) (Liu et al., 2019). In this process, it is very complicated to accurately predict the natural environment. Data mining is a computational process designed to uncover valuable insights from vast AIS datasets, revealing various historical ship motion patterns, ranging from movement pattern extraction to trajectory prediction. As a result, it has become a powerful analysis technique in maritime transport (Lei, 2016; Xiao et al., 2020; Zhou et al., 2019).

The related applications can be categorised into statistical, machine learning, and deep learning approaches. Statistical methods mainly have the Gaussian Process Regression (GPR) model, Markov Chains (MC) method, Kalman Filter (KF) method, Monte Carlo Method (MCM), similarity-based methods, etc (Li et al., 2023; Zhang et al., 2023). Specifically, the GPR model is a stochastic process with high practicability (Rong et al., 2022). On the other hand, the precision of the prediction results significantly decreases over time. The MC model is also a stochastic process model. The KF model enables short-term trajectory prediction, but its accuracy is affected by the initial conditions of the model and the ideal assumptions (Perera et al., 2012). The MCM is a probability-based statistical simulation method (Scheepens et al., 2014). There are two categories of similarity-based methods: point-level and trajectory-level (Alizadeh et al., 2021). The trajectory-level similarity is primarily measured by Dynamic Time Warping (DTW), which has revealed the drawback of being computationally intensive. In general, it is challenging to employ the above methods to handle massive trajectory data. As the volume of trajectory data increases, traditional physical or mathematical models may struggle to capture the complexity and nuances present in the data. The simplicity of these models makes them less suitable for dealing with big data, thereby requiring more advanced solutions, such as machine learning, to enhance their prediction accuracy.

The widely used machine learning approaches in the current literature include the K-Nearest Neighbors (KNN) algorithm, Support Vector Regression (SVR) method, Extreme Learning Machine (ELM) method, Random Forest (RF) method, and Bayesian Network (BN), etc (Li et al., 2023). The SVR method is a regression algorithm for predicting discrete values. It exhibits high accuracy, particularly when handling non-linearity and small sample sizes. However, it still requires attention to the parameter selection problem (Chen et al., 2021). The KNN method is a non-parametric model with inert learning, and its model structure depends on actual data (Maskooki et al., 2021). It can solve regression and classification problems by measuring the distances between different feature values. Despite its ability to effectively handle high-dimensional features, the (RF method is prone to overfitting, particularly when dealing with noisy training data (Zhang et al., 2020). The ELM, a feed-forward neural network, is frequently utilised in real-time computation. It has good generalisation and high-speed learning capabilities. As a probabilistic graphical model, BN can forecast the status of a trajectory by using the statistical properties of each ship node in a probabilistic-directed graph (Tang et al., 2020). In summary, machine learning algorithms generally suffer from achieving high-level accuracy in the presence of large amounts of data, making it challenging to solve prediction problems in complex situations.

With the significant improvement in deep learning and computer computational storage capacity (LeCun et al., 2015; Schmidhuber, 2015), it is evident that neural networks can make accurate predictions by the learned rules based on massive AIS data. Deep learning-based methods have become widespread in maritime transport (Li et al., 2023a; Zhang et al., 2022). Among numerous networks, traditional Recurrent Neural Network (RNN) models have made vital breakthroughs in processing sequential data. They however still have revealed some drawbacks in their applications in the field, such as gradient explosion and gradient disappearance) (Gao et al., 2023a, 2023b). The Long Short-Term Memory network (LSTM) and Gated Recurrent Unit (GRU) networks have been designed to solve the problems by employing a 'gated' structure. As novel optimised networks, both the Bi-directional Long Short-Term Memory (Bi-LSTM) neural network and the Bi-directional Gated Recurrent Unit (Bi-GRU) neural network can combine historical and future states to receive higher prediction accuracy compared to LSTM and GRU, respectively (Park et al., 2021). Many scholars have

explored the innovations of these methods. A new approach based on Genetic Algorithm (GA) – optimised LSTM was developed to address the issue of critical hyperparameters (Qian et al., 2022). The prediction effect of LSTM and Density-Based Spatial Clustering of Applications with Noise (DBSCAN) was proven better than that of the traditional LSTM model in AIS data (Yang et al., 2022). Time series classification and clustering can assist in prediction, which can help identify movement patterns and find abnormal trajectories (Li et al., 2020, 2018). In the relevant literature (Suo et al., 2020), GRU significantly improved computational efficiency while maintaining the same accuracy as the LSTM. A layered Bi-GRU model was introduced, showcasing impressive prediction accuracy and rapid convergence rates (Xu et al., 2022). A Bi-GRU network, leveraging a multi-headed attention mechanism, was presented to utilise the rich information embedded in the vast AIS data (Bao et al., 2022). It could actively learn the relationship between AIS data features and enhance prediction accuracy. Although showing attractiveness, the question of whether their effectiveness and hence the prediction accuracy could be further improved by their combination and taking advantage of each of them being an individual stand-alone method is still raised, wanting new experiments and tests for a clear answer. This paper aims to develop a new method to improve ship trajectory prediction accuracy and realise the real-time trajectory prediction of manned ships and MASS. It consists of two key elements: 1) a Deep Bi-Directional Information-Empowered (DBDIE) model by combining the feature information of the two bidirectional networks (i.e. Bi-LSTM and Bi-GRU) and 2) an attention mechanism for parameter optimisation.

Owing to the unique attributes of the proposed DBDIE model, this paper provides the following novel contributions.

(1) Generation of the current state of the art and research gaps in ship trajectory prediction by an in-depth literature review;
(2) Incorporation of the advantages of the Bi-LSTM and Bi-GRU models to formulate a new ship trajectory prediction method, which shows superiority over all the existing ones;
(3) Introduction of an attention machanism to determine the dynamic weights between the Bi-LSTM and Bi-GRU units to solve the optimal prediction result of the new DBDIE model;
(4) Comprehensive experiments for comparative analysis between the newly proposed method and seven established deep learning methods by using real AIS datasets from two water areas of high-level representative maritime traffic systems.

The remaining content is arranged as follows: Section 2 introduces a systematic research review of ship trajectory prediction. The preliminary and the network models are outlined in Section 3. The proposed new methodology is thoroughly presented in Section 4. Section 5 presents and analyses the experimental results, including the comparative analysis between the new model and the established ones and the discussion. Finally, the conclusion and future developments are presented in Section 6.

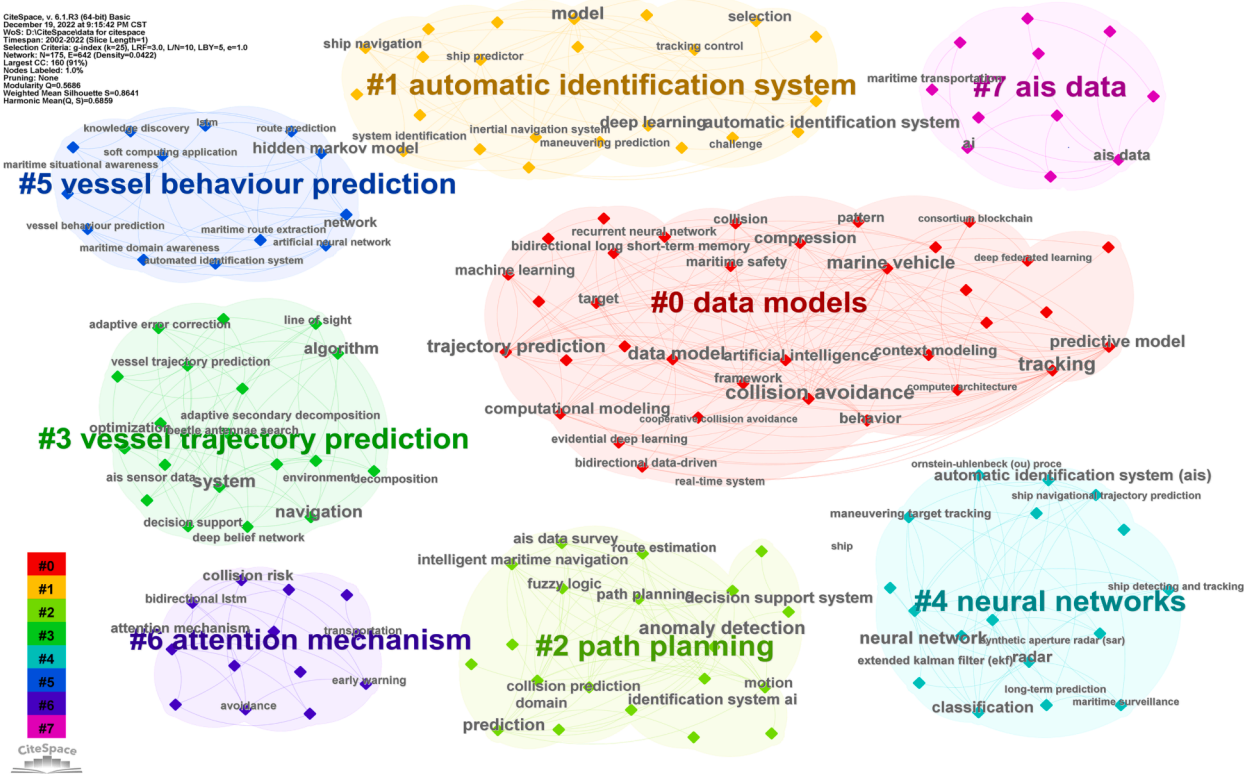

Fig. 1. The clustering analysis of keywords in ship trajectory prediction.

2. Literature review

2.1. A systematic review of ship trajectory prediction

To clearly understand the relevant research in ship trajectory prediction, the Web of Science (WoS) Core Collection database is utilised to search the published academic literature (Martin-Martin et al., 2018), in which only journal papers are included. The specific retrieval strategy uses the "or" function to concatenate "ship trajectory prediction" and "vessel trajectory prediction" as search keywords to identify all topics (e.g. the search title, abstract, and indexing). The preliminary findings consist of 1034 papers. The titles, keywords and abstract sections of the retrieval results are further screened to ensure their high relevance to their research. As a result, 103 published journal papers are selected, out of which 57 articles use deep learning methods. Each publication in the WoS database contains various information, including author, title, journal, keywords, abstract, references, etc. This information was exported to support the systematic review and comprehensive literature analysis.

A keyword clustering method is employed to aggregate similar research topics within the ship trajectory prediction area, forming clusters of interconnected networks. This approach provides a more intuitive way to identify the leading techniques and research directions in the current field (Chen, 2006). The CiteSpace software (Synnestvedt et al., 2005) is applied to cluster closely related keywords algorithmically in the selected 103 papers. The results are displayed in Fig. 1, where eight categories with different titles and nodes are generated to visualise their similarities and differences. Each category includes various keywords with different frequencies of occurrence. It is noted that the most frequently occurring keyword within each category is highlighted in coloured font, serving as the title of that cluster. The nodes and corresponding labels in each category are identified using the black font in the upper corner.

Researchers have focused on the applications (e.g. vessel behaviour prediction, vessel trajectory prediction, and path planning), AIS, and methods of trajectory prediction (e.g. data models, neural networks, and the attention mechanism) in Fig. 1. Among the primary techniques, the applications of deep learning models and an attention mechanism have attracted enormous attention. Although having its emphasis, each clustering result is not independent, having some similar keywords, including AIS data, unique algorithms or models, and the construction of a complete framework as the links. For instance, category #0 contains a large number of keywords about data models. The keywords in category #6 focus on applying the attention mechanism.

Moreover, the timeline analysis of the closely related keywords in the 103 literature collection is conducted using the CiteSpace software. The clustered keywords are expanded in chronological order, and the trend of keywords under each category can be seen in Fig. 2. The timeline focuses more on the period and the process of change of a research topic under a cluster.

Overall, deep learning, AIS data, and marine vehicles are among the top three categories with a relatively large number of topics to discuss. They have been in the mainstream of research for over 15 years, from 2007 to 2022. Categories #3–#7 mainly focus on the

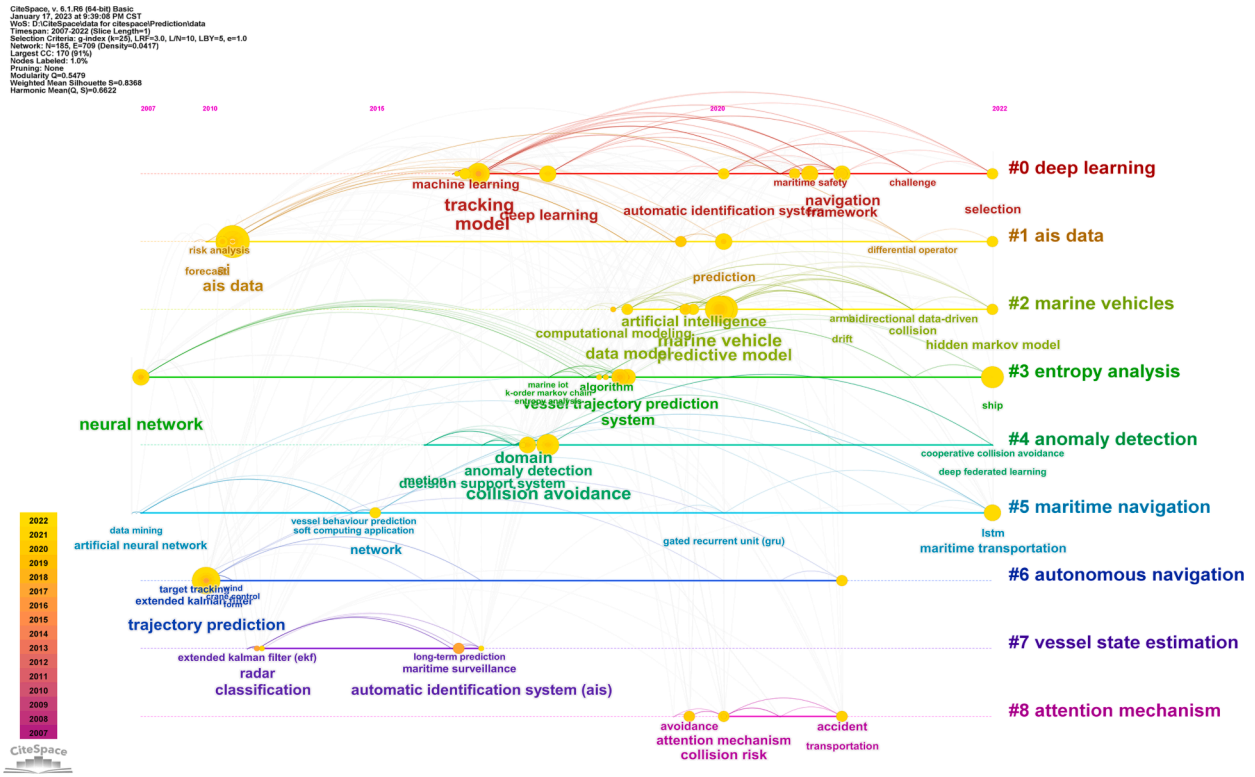

Fig. 2. The timeline analysis of keywords in ship trajectory prediction.

applications of trajectory prediction. The techniques have evolved significantly in their developments, ranging from machine learning strategies to deep learning methods. In all categories, time series analysis and the attention mechanism emerge as the most frequently used methods in deep learning. Following the architecture analysis in the field, the contextual insights on using machine learning methods in ship trajectory prediction are further investigated by summarising the in-depth methodological analysis of the machine learning-related papers.

The statistically-based methods can obtain good prediction results and are computationally efficient for handling small datasets. The ship's motion includes two directions: horizontal and vertical (Rong et al., 2019). The horizontal direction of the lateral motion is simulated by the Gaussian process, and the acceleration is used to determine the longitudinal direction. However, as time advances, the prediction accuracy of the outcomes diminishes considerably. A new algorithm was proposed based on a grid-level structure using multiple navigation-related parameters and K-order multivariate MC for long-term ship trajectory prediction (Liu et al., 2019). An Extended Kalman Filter (EKF) method was put forward to estimate a ship's future navigational state (Perera et al., 2012).

Among kinds of machine learning-based methods, an SVR-based trajectory prediction model was designed using ship speed, heading, time-stamp, latitude and longitude as sample features in AIS data (Liu et al., 2019). By optimising model parameters, the Adaptive Chaotic Differential Evolution (ACDE) algorithm was developed to accelerate convergence. KNN was introduced for estimating the ship's future behaviour. Maskooki et al. (2021) conducted experiments based on AIS data from the Gulf of Finland, requiring several hours in advance with reasonable accuracy and verifying that the method could predict accurately within minutes. Wang et al. (2022) compared several widely used data-driven models and chose the random forests, with the innovation of introducing potential information about the engine state into the model learning.

In conclusion, both statistical and machine learning methods can be somewhat effective in short-term forecasting and are computationally efficient. However, the models are typically constrained and susceptible to the initial state and ideal condition assumptions. As we approach a future marked by intricate interactions between manned ships, MASS and the associated vast traffic, there is an imperative need for advanced methods to improve trajectory prediction accuracy.

2.2. Research progress of trajectory prediction based on deep learning

Deep learning methods have powerful learning and analysis capabilities. Therefore, their applications to trajectory prediction tasks have become an important direction in maritime transport. A collection of 57 papers using deep learning methods is selected for the timeline analysis. The changing research focuses in the last four years (i.e. 2019–2022) are illustrated in Fig. 3. The node size corresponds to the frequency of keywords over time, as depicted in the graph. Within category #1, the deep learning node is the most prominent, indicating that since 2020, trajectory prediction methods based on deep learning have gained considerable attention.

Among six clustering labels, the keywords in category #0 (i.e. deep learning) change most frequently, which reflects the prioritised research activity in this field. Categories #2–#4 are specific strategies and methods of deep learning in trajectory prediction, which have received continuous attention and are analysed separately. Specifically, frequently used methods are various recurrent neural networks. Trajectory prediction also assists the development of automated technologies for unmanned ships. Meantime, the emphasis

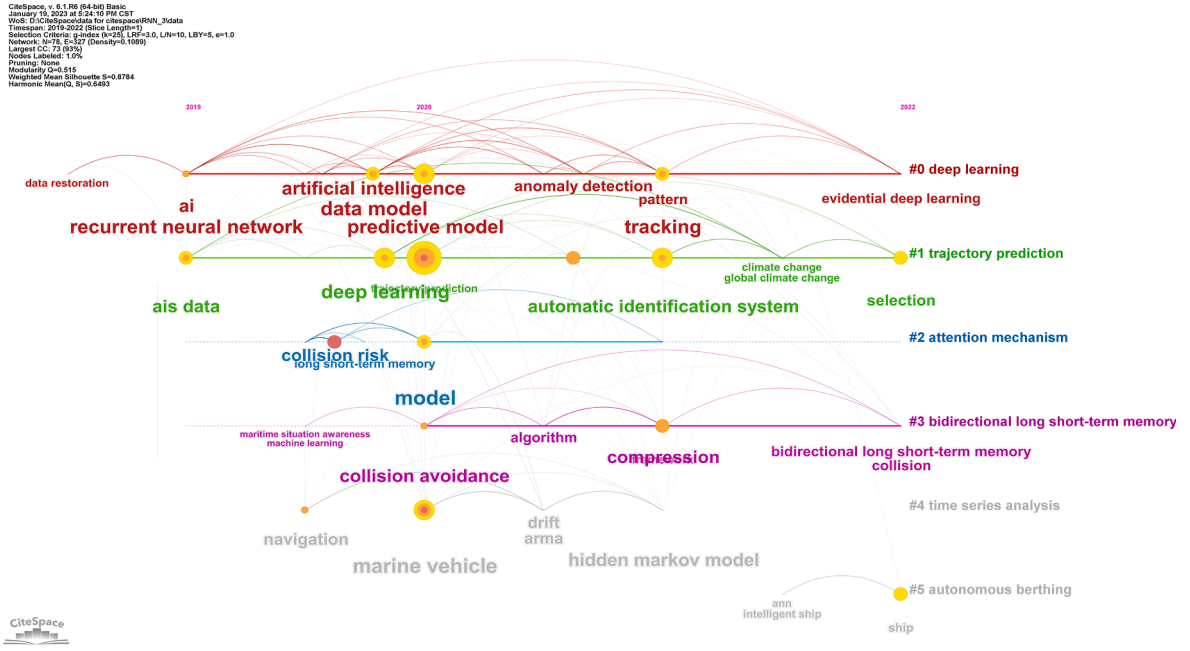

Fig. 3. The timeline analysis for keyword changes by deep learning methods.

of research in different years also varies. The research in 2019 is still relatively homogeneous. In contrast, the keywords are more prosperous, reflecting various applications and models for trajectory prediction after 2020. A detailed description of the deep learning methods involved in recent years is provided below.

LSTM is one of the most common models used for ship trajectory prediction in deep learning methods. Yang et al. (2022) combined the DBSCAN with the LSTM model for ship prediction, which could provide better prediction performance than RNN. Through a recursive mechanism, it was demonstrated that a Context-aware Long Short-Term Memory (CLSTM) network might increase prediction accuracy while preserving logical coherence (Mehri et al., 2021). Some researchers also actively explored the application of the LSTM model in navigation prediction (Ma et al., 2022, 2021; Venskus et al., 2021). A novel framework was developed by combining a Bi-LSTM network and the attention mechanism (Ma et al., 2020). It outperformed the traditional LSTM in terms of stability and accuracy as key information relevant to the risk prediction task could be emphasised. A Bi-directional Long Short-Term Memory Mixture Density Network (BLSTM-MDN) model was introduced to analyse the potential distribution of ship trajectories and produce better results in complex scenarios (Sorensen et al., 2022).

GRU also has excellent capability in handling time series data. A GRU model was introduced by Suo et al. (2020), and the experimental results showed that it could increase computational efficiency with similar prediction accuracy compared to LSTM. A GRU model with the attention mechanism and an AutoRegressive (AR) model were combined to predict the trajectories (Zhang et al., 2021). The attention mechanism was designed to set different weights for features. The AR model and the output from the attention mechanism were combined to predict the information on latitude and longitude at the current timestep. A multi-headed attention mechanism and a bi-directional gated recurrent unit were combined to construct a highly accurate and reliable prediction model, which was easy to implement (Bao et al., 2022).

Kim and Lee (2018) proposed a hybrid deep learning framework based on the Convolution Neural Network (CNN) and Fully Connected Neural Network (FCNN), which could learn the movement patterns of ships. FCNN was used to obtain more hidden features from other valuable information (e.g. Estimated Time of Arrival (ETA), length, destination, and ship types). CNN has also been used to extract multi-scale features (Zhang et al., 2021). Based on an adversarial system and training competitively, a Generative Adversarial Network (GAN) with Attention Module and Interaction Module (GAN-AI) could be better fused to predict the trajectory (Wang and He, 2021). An extended Seq2Seq model was introduced to realise the short-time prediction (You et al., 2020). In addition to maintaining the sequential linkages between trajectory points, a GRU network that encoded spatiotemporal historical sequences as a context vector also addressed the gradient descent problem. As a decoder, a GRU network generated target trajectory location sequences. Murray and Perera (2020) applied a novel bilinear autoencoder method to forecast the future trajectories of selected ships and quantified the uncertainty of ship position. Huang et al. (2022) developed a model incorporating discrete meteorological data using TripleConv-Transformer to extract ocean-going ships' motion information deeply.

Deep learning-based methods, in general, have the ability to extract valuable information and exhibit strong learning capabilities, making them well-suited for handling massive AIS data. However, the question of whether the existing deep learning methods, either individually or in combination, can deliver the best performance in terms of reliability and accuracy for AIS data-driven trajectory prediction remains unanswered.

2.3. Research gaps

Although many deep learning approaches have been applied in ship trajectory prediction, previous studies have highlighted certain challenges encountered during their applications.

Firstly, there is a need to improve the scalability of these models across different regions. Prediction performance tends to degrade when a deep learning-based prediction model is transferred to a different geographical area. Consequently, it remains a challenging task to design a more adaptive and general cross-regional model.

Secondly, existing studies have predominantly focused on the individual use of these methods. The performance achieved by using them collectively has not been thoroughly benchmarked against their individual counterparts. The question as to how to effectively leverage two or more models to overcome their inherent limitations remains unanswered. It is possible to enhance prediction accuracy through the fusion of multiple methods. However, in this combination process, a new challenge arises regarding how to properly balance the contributions from each individual method to ensure the robustness of the combined approach.

More specifically, the current theoretical state of the art for combined deep learning methods is more represented by the second-tier solutions in which the classical individual deep learning methods are combined and/or further developed. There are no studies upon the authors' best knowledge, focusing on the new third-tier solutions in which two or more second-tier solutions are combined to optimise their individual strengths collectively. This study fulfils the gap and initiates the pioneering third-tier solutions, namely the combination of Bi-LSTM, Bi-GRU, and an attention machanism. This not only guides the evolution of deep learning methods in general steers their specific implementations in ship trajectory prediction.

To address these issues, an integrated model and an attention mechanism have been identified as promising solutions. They have been incorporated to develop a novel DBDIE method, as elaborated in Sections 3 and 4.

3. Preliminary

This section delves into the theoretical frameworks and structures of seven state-of-the-art deep learning models: RNN, LSTM, GRU, Bi-LSTM, Bi-GRU, Seq2Seq, and Transformer. Concurrently, the design process of these algorithms using the Pytorch framework is presented through pseudocode.

3.1. State-of-the-art deep learning methods

3.1.1. RNN

RNN takes sequence data as input and output, comprising the input layer, the output layer, and the hidden layer. Meanwhile, the relationship between sequences can be well utilised by introducing state variables through the connected hidden layers to store history information. Fig. 4 illustrates the structural layout of RNN.

At the moment t, s_{t-1} and x_t are the input. o_t can be calculated as the output. Meanwhile, s_{t-1} is passed to the next moment so that s_t can get the previous information. A linear layer is added after the basic RNN unit for the output. RNNs are effective in handling short-sequence tasks. However, when it comes to establishing associations between long sequences, issues like gradient disappearance or gradient explosion during backpropagation calculations can arise, ultimately resulting in the failure of network training.

3.1.2. LSTM

In contrast to RNN, LSTM is better at capturing the relationships between lengthy sequences, alleviating the gradient vanishing or explosion issue. There are three types of gates that control information flow: input gates, forgetting gates, and output gates. A memory unit is also added to the LSTM cell to preserve historical states. The architecture of the LSTM model is presented in Fig. 5.

At the moment t, x_t, h_t, and c_t are the input, output, and state vector of the LSTM unit, respectively. Similarly, h_{t-1} and c_{t-1} are the output and state vector at the moment $t-1$, respectively. σ can convert a value to [0,1], while $tanh()$ can compress real value to [-1,1]. The output gate O_t can be calculated by

$$O_t = \sigma(W_o \cdot [h_{t-1}, x_t] + b_o), \tag{1}$$

where W_o and b_o are the weight matrix and bias vector of the output gate, respectively.

Then the output of the LSTM cell can be modelled as

$$h_t = O_t \times tanh(c_t). \tag{2}$$

A linear layer is added after the basic LSTM unit for the output.

3.1.3. Bi-LSTM

LSTM can only make predictions on sequence information from previous moments. The output of the present moment, however, may occasionally be connected to the status of the future. Although the internal structure of Bi-LSTM is the same as that of LSTM, Bi-LSTM has a backward and forward layer to fully consider contextual information. The effectiveness of time series prediction is improved by concatenating the forward and backward output vectors. The schematic diagram of Bi-LSTM is presented in Fig. 6.

$\overrightarrow{h}_t$ and $\overleftarrow{h}_t$ store the output of the LSTM cells at the moment t in the forward and backward layers, respectively. Ultimately, the outputs from the forward and backward layers are integrated and processed at each instance to produce the final result. The specific calculation models are listed in Eqs. (3)–(4).

$$h_t = \overrightarrow{h}_t \oplus \overleftarrow{h}_t, \tag{3}$$

$$o_t = W_t \cdot h_t + b_t, \tag{4}$$

where o_t represents the output at the moment t. W_t and b_t indicate the weight and deviation vector of the network, respectively. A linear layer is added after the basic Bi-LSTM unit for the output.

3.1.4. GRU

GRU is more computationally efficient than LSTM by improving the unit's structure. The update gate can change the state of the memory unit, which merges the forgetting and input gates of LSTM. A reset gate is designed to decide whether to ignore the previous state of the memory unit. Its schematic diagram is shown in Fig. 7.

The state of the update gate R_t, the reset gate Z_t, and the status of the current memory unit $\tilde{h}_t$ can be calculated by

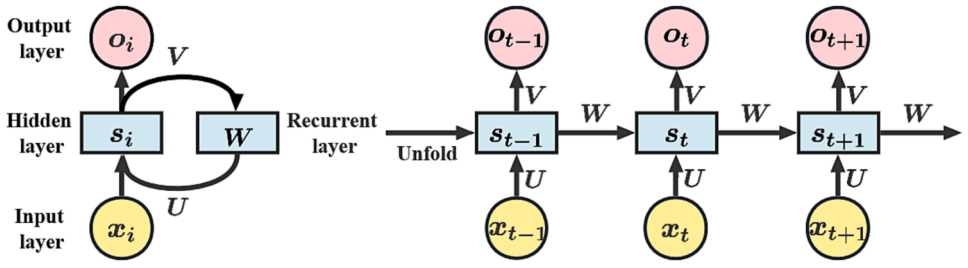

Fig. 4. The overview of the RNN structure.

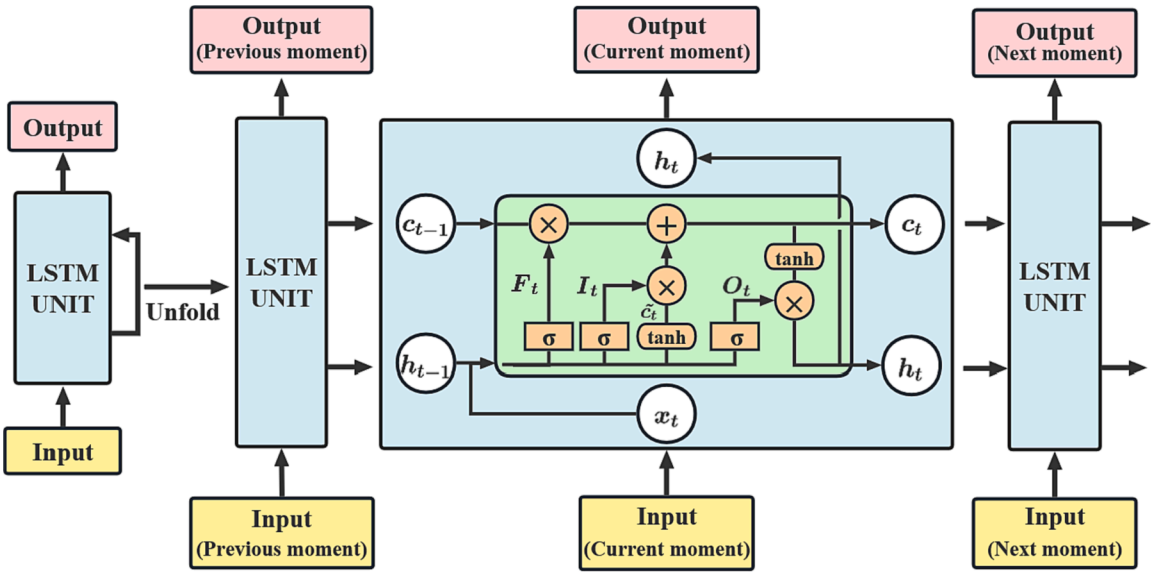

Fig. 5. The overview of the LSTM structure.

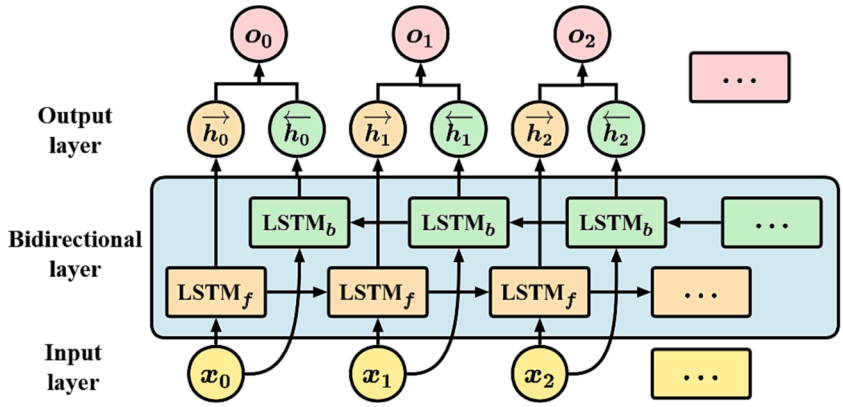

Fig. 6. The overview of the Bi-LSTM structure.

$$R_t = \sigma(W_r \cdot [h_{t-1}, x_t]), \tag{5}$$

$$Z_t = \sigma(W_r \cdot [h_{t-1}, x_t]), \tag{6}$$

$$\widetilde{h}_t = tanh(W_{\widetilde{h}_t \cdot [R_t \times h_{t-1}, x_t])}, \tag{7}$$

where W_r and $W_{\widetilde{h}_t}$ are the weight matrix of the reset gate and the current memory unit, respectively.

During the update phase, both 'memory' and 'forgetting' functions are executed concurrently. If Z_t approaches 1, the output corresponds to the current memory unit's candidate state $\widetilde{h}_t$. Conversely, when Z_t is nearing 0, the output aligns with $\widetilde{h}_t$ from the prior time step. The model is shown below.

$$h_t = (1 - Z_t) \times h_{t-1} + Z_t \times \widetilde{h}_t. \tag{8}$$

A linear layer is added after the basic GRU unit for the output.

3.1.5. Bi-GRU

Bi-GRU takes into account the continuity of sequential data at past and future moments. It does not change the basic structure of GRU but also applies the same calculation process twice in different directions. Then it splices and calculates the results obtained from two layers as the final output. The visualised framework is displayed in Fig. 8.

Bi-GRU can facilitate feature extraction by combing results to get the final output o_t. The final results can be formulated by

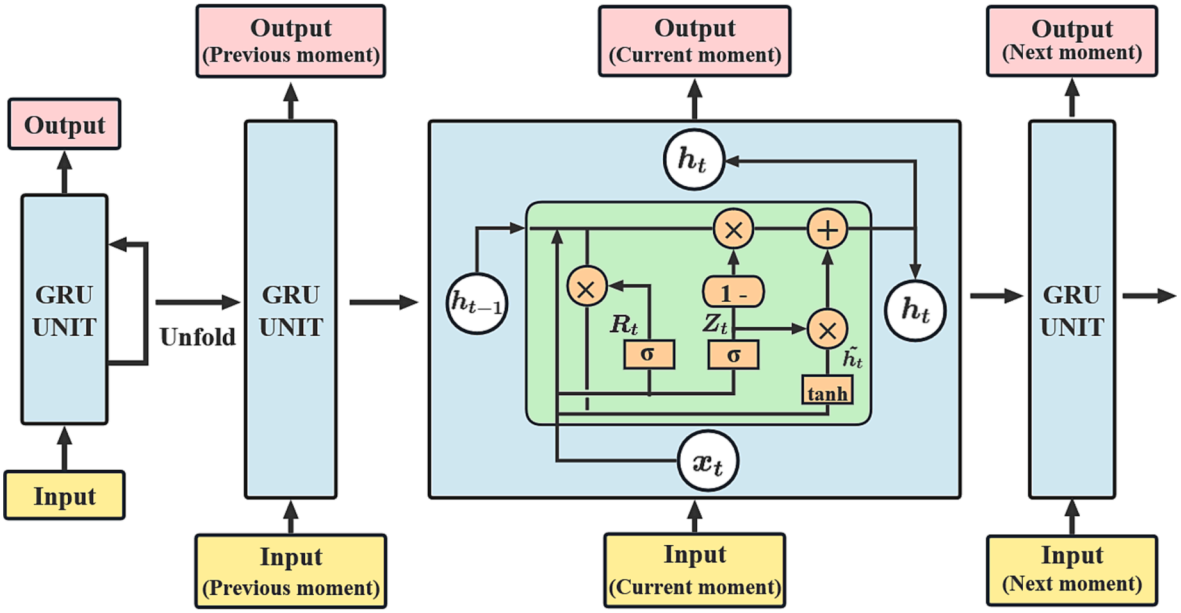

Fig. 7. The framework of the GRU structure.

$$h_t = \overrightarrow{h}_t \oplus \overleftarrow{h}_t, \tag{9}$$

$$o_t = W_t \cdot h_t + b_t. \tag{10}$$

A linear layer is added after the basic Bi-GRU unit for the output.

3.1.6. Seq2Seq

The Seq2Seq model is structured around two primary elements: the encoder and the decoder. The encoder processes the input sequence into a uniform-length context vector, with its concluding hidden state serving as the context for the decoder. The decoder then takes this vector to produce the intended target sequence. Both components are built upon RNN frameworks. A visual representation of the Seq2Seq model can be found in Fig. 9.

3.1.7. Transformer

The primary innovations of the Transformer model include the self-attention mechanism and positional encoding. The self-attention mechanism allows the model to establish relationships between any two elements in the input sequence, enabling parallel computation and enhancing training efficiency. On the other hand, positional encoding assigns unique position information to each input element, enabling the model to handle the positional order of the sequence. The structure of the Transformer model is presented in Fig. 10.

The Transformer model's calculation process involves embedding the input sequence and adding positional encoding to introduce position information. The encoded sequence is then processed through self-attention and feed-forward neural network layers in the encoder, and similar operations are performed in the decoder, including self-attention and encoder-decoder attention. The decoder's output is projected into a probability distribution over the vocabulary for generating the target sequence. The model is trained using backpropagation and optimisation to minimise errors between its prediction and the real value. During inference, the decoder

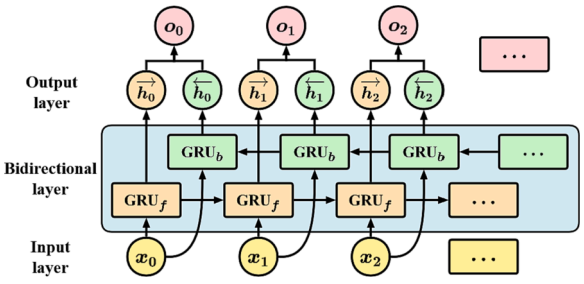

Fig. 8. The visualised framework of the Bi-GRU method.

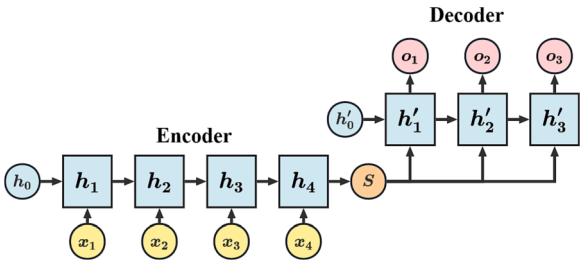

Fig. 9. The schematic diagram of the Seq2Seq method.

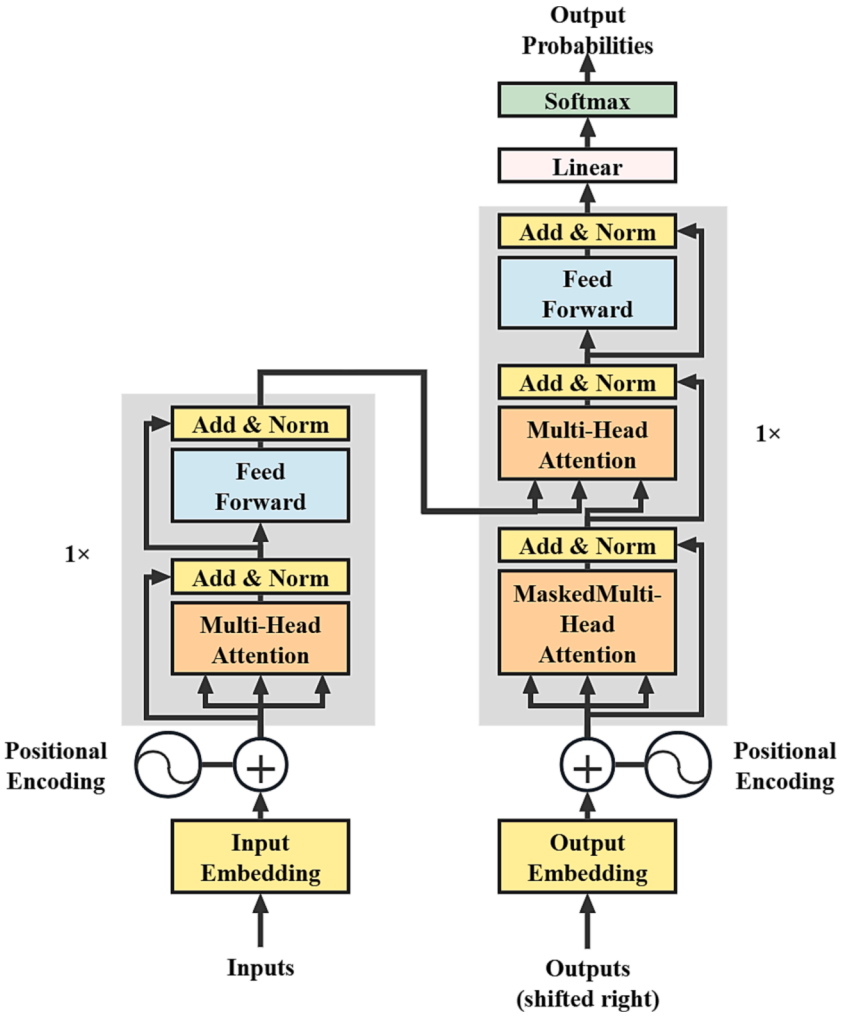

Fig. 10. The schematic diagram of the Transformer method.

generates subsequent tokens in an autoregressive manner.

3.2. Time complexity comparison of different methods

Following the aforementioned theoretical analysis and algorithmic overview, Table 1 lists the time complexities of the seven different models, giving a comparative perspective. Within the table, T stands for the length of the sequence, d represents the dimension of the model's hidden layer, and l indicates the number of layers in the Transformer model. Time complexity analysis offers insights into the computational demands and scalability of various models in relation to the size of the input. RNNs, having the least time complexity, are best suited for shorter sequences and less computationally intensive tasks. LSTMs and GRUs, while more

computationally demanding due to their complex gating mechanisms, can handle longer sequences. Bi-directional models like Bi-LSTM and Bi-GRU provide more contextual information by processing sequences in both directions, but this comes at a higher computational cost. Seq2seq models, like Bi-LSTMs, require significant resources due to their dual LSTM/GRU structures, but they perform well in tasks needing comprehensive sequence understanding. Lastly, the Transformer model, while effective in managing long-range dependencies and offering better parallelization, can be computationally expensive for extended sequences. The optimal model choice depends on the specific task, available computational resources, and the nature of the input sequences.

To summarise, both LSTM and GRU are effective solutions to address the issue of gradient disappearance or explosion in RNN. The structure of the LSTM is more complex and computationally slow. On the other hand, GRU is a modified version of LSTM with improved internal structure and computational efficiency. Two bidirectional networks (i.e. Bi-LSTM and Bi-GRU) are constructed based on LSTM and GRU to capture more valuable features from sequence data. Seq2Seq model consists of an encoder-decoder architecture, which is well-suited for handling sequential data with variable-length inputs and outputs. The transformer model relies on self-attention mechanisms to capture relationships between different words or elements in a sequence, which can model long-range dependencies.

This paper's primary objective is, for the first time, to integrate and enhance two bidirectional networks and subsequently determine the optimal weights using the attention mechanism, achieving improved prediction accuracy and yielding optimal performance.

4. Methodology

When solving the trajectory prediction task, a single model often suffers from the disadvantages of unstable prediction results and insufficient generalisation ability. The existing studies mainly focus on models, data, and optimisers. In this paper, an integrated model is developed from the perspective of enhanced networks and the optimisation of the attentional mechanism. It aids to address the limitations of individual models and enhance the overall ship trajectory prediction accuracy.

To achieve this, the proposed integrated model combines the strengths of Bi-LSTM and Bi-GRU models and takes into account variations in integrated predictions. By strategically combining the results of each model, a fusion network is obtained. The integrated network incorporates both Bi-LSTM and Bi-GRU units to recognise their advantages in analysing sequence information. Additionally, an attention mechanism is introduced to automatically determine the optimal weights based on predicted results. The structure of the proposed DBDIE model is displayed in Fig. 11. DBDIE comprehensively incorporates several key technologies, including bidirectional networks, attention mechanisms, and feature fusion, seamlessly blending them within a unified framework to realise improved ship trajectory prediction accuracy. It hence makes significant methodological contributions to the field. This fusion empowers the model with advanced representation learning and generalisation capabilities, enabling it to effectively learn from historical data and predict ship trajectories accurately.

$\overset{\frown}{h}_t$ and $\overset{\frown}{h}_{t-1}$ are the state vectors of the memory unit in the Bi-GRU cells at the moment t and $t-1$, respectively. $\overset{\smile}{h}_t$ and $\overset{\smile}{h}_{t-1}$ indicate the state vectors of the memory unit in the Bi-LSTM cells at the moment t and $t-1$, respectively. The computational procedure of the proposed DBDIE algorithm is shown in Eqs. (11)–(17).

(1) At the moment t, the sequence information is calculated by the Bi-GRU unit and the Bi-LSTM unit to obtain $\overset{\frown}{h}_t$ and $\overset{\smile}{h}_t$, respectively. Then $\overset{\frown}{h}_t^{'}$ and $\overset{\smile}{h}_t^{'}$ are obtained through a non-linear layer. The above two results are then directly concatenated together and used as input for the next moment (i.e. h_t).

$$\overset{\frown}{h}_t^{'} = tanh(W_g \cdot \overset{\frown}{h}_t + b_g), \tag{11}$$

$$\overset{\smile}{h}_t^{'} = tanh(W_l \cdot \overset{\smile}{h}_t + b_l), \tag{12}$$

$$h_t = \overset{\frown}{h}_t^{'} \oplus \overset{\smile}{h}_t^{'}, \tag{13}$$

where W_g and b_g is the weight matrix and bias vector of the Bi-GRU unit, respectively. Meantime, W_l and b_l is the weight matrix and bias vector of the Bi-LSTM unit, respectively.

(2) Compute the weight parameters of the two networks using the attention mechanism (i.e. β).

Table 1
The overall comparison of seven models.

Model	Time complexity	Model	Time complexity
RNN	$O(T*d^2)$	Bi-GRU	$O(T*6d^2)$
LSTM	$O(T*4d^2)$	Seq2Seq	$O(T*8d^2)$
GRU	$O(T*3d^2)$	Transformer	$O(l*T*d^2)$
Bi-LSTM	$O(T*8d^2)$		

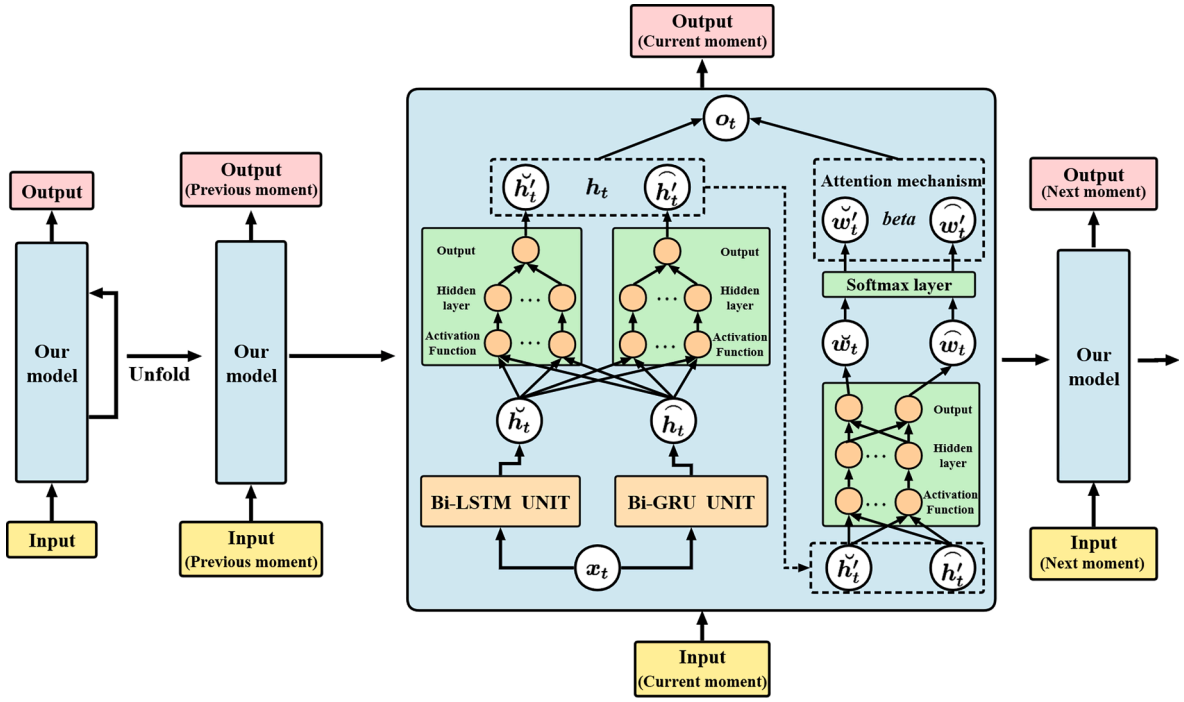

Fig. 11. The flowchart of the proposed DBDIE model structure.

$$\overset{\frown}{w}_t^{'} = \sigma(tanh(W_t \cdot \overset{\frown}{h}_t^{'} + b_t)), \tag{14}$$

$$\overset{\smile}{w}_t^{'} = \sigma(tanh(W_t \cdot \overset{\smile}{h}_t^{'} + b_t)), \tag{15}$$

$$\beta = \overset{\frown}{w}_t^{'} \oplus \overset{\smile}{w}_t^{'}, \tag{16}$$

where W_t and b_t is the weight matrix and bias vector using the attention mechanism, respectively.

(3) Calculate the final fusion result (i.e. o_t).

$$o_t = \beta \cdot h_t. \tag{17}$$

The algorithm is described in pseudocode below.

(*continued on next page*)

(*continued*)

Input: A training set $Traj = (lon_i, lat_i), i = 1, 2, \cdots, n$ and learning rate η

Output: A well-trained DBDIE model

1: bi_lstm = Bi-LSTM(input_size, hidden_size, num_layers, bidirectional, dropout);
2: seq_1 = Sequential(Linear(input_features = hidden_size * 2, output_features = 128), tanh(),
Linear (input_features = 128, output_features = output_size));
3: bi_gru = Bi-GRU(input_size, hidden_size, num_layers, bidirection, dropout);
4: seq_2 = Sequential(Linear(input_features = hidden_size * 2, output_features = 128), tanh(),
Linear (input_features = 128, output_features = output_size));
5: project = Sequential(Linear(in_features = 2, out_features = 16, bias = True), tanh(),
Linear(in_features = 16, out_features = 1, bias = True));
6: **For** epoch = 1: N **do**:
7: **For all** (lon_i, lat_i) **in** $Traj$:
8: bi_gru_out, hidden = bi_gru((lon_i, lat_i));
9: seq_1_out = seq_1(bi_gru_out);
10: bi_lstm_out, hidden = bi_lstm((lon_i, lat_i));
11: seq_2_out = seq_2(bi_lstm_out);
12: Stack the results of seq_1_out and seq_2_out in the direction of the column: features;
13: beta = softmax(project(features), dim = 1);
14: output = (beta * features).sum(dim = 1);
15: Compute the error between the output and tag value;
16: Backpropagation of loss: loss.backward();
17: Update parameters with optimiser: optimiser.step();
18: **End for**
19: **End for**

5. Experimental results and analysis

The practicality and effectiveness of the DBDIE method are verified through comparative experiments in the real AIS datasets collected from two representative water areas. Firstly, eight models are trained using the processed AIS data with the same

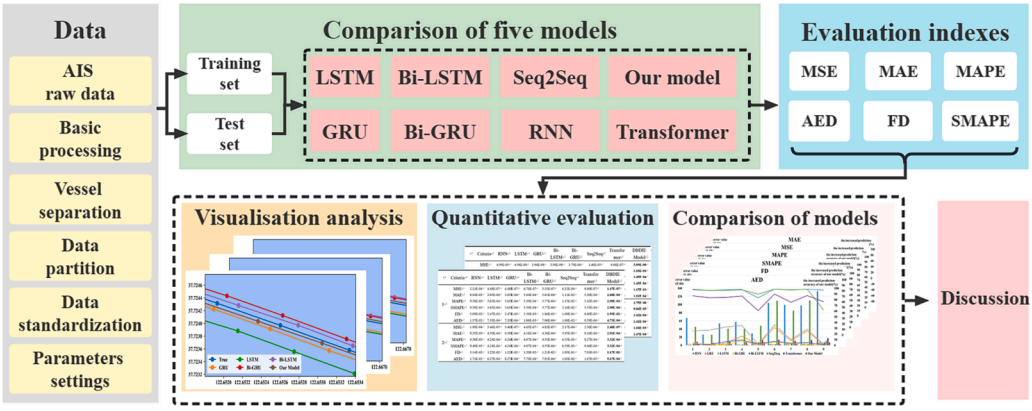

Fig. 12. The flowchart of the proposed ship trajectory prediction framework.

hyperparameters. The accuracy of the novel DBDIE method and the seven classical ones is then quantitatively evaluated by six indexes that are the most commonly used in different literature, including Mean Square Error (MSE), Mean Absolute Error (MAE), Mean Absolute Percentage Error (MAPE), Symmetric Mean Absolute Percentage Error (SMAPE), Fréchet Distance (FD), and Average Euclidean Distance (AED). Moreover, the visualisation analysis of the predicted trajectories and the ground truth is analysed and compared to highlight the performance of the eight methods and demonstrate the effectiveness of the proposed DBDIE model. Furthermore, the quantitative evaluation of the six index values is used to compare their performance from the error rate and the increased accuracy. As a result, it reveals the essence of each model and verifies the effectiveness of the proposed DBDIE model. Finally, the valuable analysis of the proposed DBDIE model is received to guide future development. The flowchart of the proposed ship trajectory prediction framework is shown in Fig. 12.

5.1. Experimental datasets

Two typical ship trajectory datasets were collected from the Chengshan Jiao (CJ) water area in January 2018 and the Caofeidian Port (CP) water area in July 2017 for model training and testing. The experiments are conducted using 64-bit Windows 10 on a 3.10 GHz Intel Core i5-11300H CPU, GPU, and 16 GB of RAM and are programmed using Python.

The CJ water area is the essential route for ships entering and leaving the Bohai Sea and the ports in the northern Yellow Sea. As one of the main routes of maritime traffic in China, it is characterised by dense ship traffic and a complex climate and sea state. The total number of ships sailing and operating in this water area reaches more than 800,000 per year. Meantime, the high ship density and numerous crossings increase the risk of collisions and groundings. The experiments are conducted in the CJ water area with a study area of 122°58′–123°17′E and 37°16′–37°75′N. The dataset has 2000 trajectories with 1,492,889 time-stamped points after data cleaning, displayed in Fig. 13.

The CP water area has the most intensive traffic flow in the western part of the Bohai Sea. Its layout is logical and possesses exceptional economic and geographical advantages for establishing a major deep-water port. The second experiment is conducted based on the AIS dataset from the CP water area, with the study area of 118°25′–118°92′E and 38°71′–39°11′N. The dataset contains 1219 trajectories with 1,644,987 time-stamped points after data cleaning, shown in Fig. 14.

5.2. Experimental setting

5.2.1. Data normalisation

Data normalisation ensures that there are no dimensional issues between the data. In this paper, the longitude and latitude data of the original trajectories are processed using the min–max normalisation method. The raw data is mapped to the interval $[0, 1]$ and then served as input data. The neural network output processed in the interval from 0 to 1 is back-normalised and mapped to the original range level of the sample sequence data. The specific calculation process is presented in Eqs. (18)–(19).

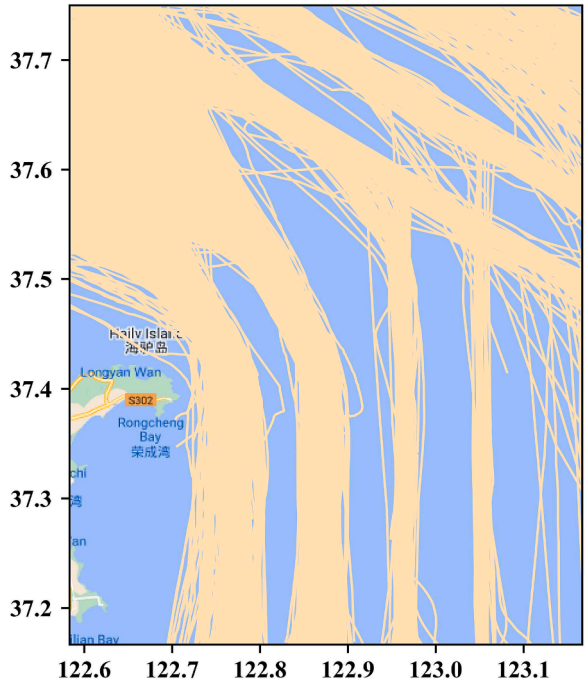

Fig. 13. Visualisation of the dataset in the CJ water area.

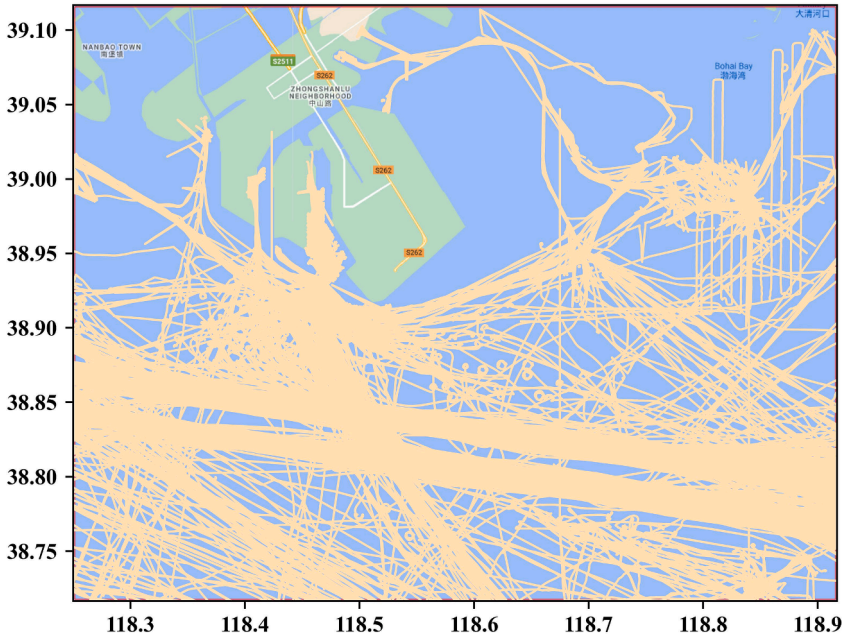

Fig. 14. Visualisation of the dataset in the CP water area.

$$X_{std} = \frac{x - x_{\min}}{x_{\max} - x_{\min}}, \tag{18}$$

$$X_{scaler} = x_{std}(x_{\max} - x_{\min}) + x_{\min}, \tag{19}$$

where $x_{\min}$ and $x_{\max}$ are the smallest and largest values of the original trajectory data, respectively. X_{std} indicates the normalised sequence data. X_{scaler} expresses the denormalised sequence data, and x represents the raw data.

5.2.2. The training and testing dataset

After the data has been processed, 80 % of the dataset is served as a training set for further identifying parameters, while the remaining 20 % is used as a testing set for verifying the accuracy. One trajectory is selected from each cluster obtained by the clustering analysis in the test dataset separately to generate the final test dataset (Li et al., 2022).

The training and test datasets process the trajectory latitude and longitude information of four consecutive time points into a vector, and utilise the data of the following time point as the prediction label. The above process is described in Eq. (20).

$$f[x_5, y_5] = f([x_1, y_1], [x_2, y_2], [x_3, y_3], [x_4, y_4]), \tag{20}$$

where x and y represent the trajectory latitude and longitude value of one point, respectively.

5.2.3. Model and hyperparameter settings

Pytorch is used to help design the model for the experiments. The choice of hyperparameters is also crucial to train the neural network. The best combination of parameters in Table 2 is obtained through extensive experimental comparison and argumentation. Experiments 1 and 2 refer to the experiments conducted in the CJ and CP water areas, respectively.

Regardless of the model used during the experiment, the consistency of the above hyperparameters is ensured to achieve comparative results. Thus, the performance of each model is finally compared through statistical error and improved accuracy. The convergence counts of different models during the two experiments are shown in Table 3.

5.2.4. The adaptive weight calculation

The optimal weights of the Bi-LSTM and Bi-GRU units in the proposed DBDIE model are adaptively calculated and obtained by an attention mechanism, as shown in Table 4. Given that the performance of Bi-GRU is better than that of Bi-LSTM during the

Table 2
The relevant hyperparameters combination.

Experiment	Learning Rate	Training times	Batch size	Input dimensions	Hidden layers	Output dimensions	Network layers
1 and 2	0.0001	300	75	2	256	2	1

Table 3
Counts of convergence of the experiments.

Experiment	RNN	LSTM	GRU	Bi-LSTM	Bi-GRU	Seq2Seq	Transformer	DBDIE
1	130	150	130	250	210	190	230	200
2	170	180	160	270	260	230	270	250

Table 4
The optimal weight of two network units.

Average weights in different water areas	Bi-LSTM unit	Bi-GRU unit
CJ water area	0.479	0.521
CP water area	0.487	0.513

experiments, its weights are slightly larger than those of Bi-LSTM based on the results from the attention mechanism. The adaptive weight calculation can guarantee better prediction performance compared to the other four models.

5.2.5. Comparison of training time across different methods

According to the above theoretical analysis and algorithm comparison, the comparative differences in each iteration in the seven models are listed in Table 5. This table delivers a numerical overview of the computational expense associated with each of the seven models, thereby aiding in the selection of the most suitable model considering the available computational resources and task prerequisites. These seven models act as benchmarks in this comparative experimental setup.

5.2.6. Model performance validation

The prediction performance evaluation of the proposed DBDIE model involves observing and analysing the loss function descent curves alongside those of the other seven models across two distinct water areas. It also includes a comparison of the training and validation loss function values. The graphs illustrating loss reduction, as depicted in Fig. 15, showcase a consistent downward trend in loss values for both water areas. On the horizontal axis, the number of training epochs is represented, while the vertical axis denotes the corresponding loss values. A comparison between Fig. 15 (a) and (b) clearly demonstrates that the proposed DBDIE model achieves rapid convergence.

The advantages of rapid convergence encompass a multitude of factors in the proposed DBDIE model. Firstly, it optimises the utilisation of time and computational resources by achieving a stable performance level through fewer training iterations. This efficacy facilitates accelerated cycles of experimentation and iteration, permitting swift assessments of diverse model architectures, hyperparameters, and data preprocessing techniques. Additionally, the diminished risk of overfitting, which accompanies fast convergence, bolsters the model's adaptability to unfamiliar data instances, thereby fostering confidence in its generalisation capacities. This flexibility in responding to shifts in data distribution or task prerequisites is pivotal in sustaining the model's predictive effectiveness in dynamic scenarios. In operational settings, the ability to rapidly converge equips the model to promptly assimilate new data, thus heightening the efficiency and reliability of real-time decision-making systems. However, it's crucial to acknowledge that the pursuit of rapid convergence should be balanced with the model's ability to capture essential data features, ensuring both optimal and stable generalisation performance.

Therefore, the comparative outcomes of the training and validation loss curves, as produced by the DBDIE model, are portrayed in Fig. 15 (c) and (d), signifying the model's effective assimilation of data features, thereby enabling preliminary predictions on both datasets. As the training process advances, the model's loss values consistently decrease for both the training and validation sets, indicating its capacity to capture intricate data patterns and mitigate noise within the training set. Around the 250–300 epoch range in both water areas, the gap between the losses of the training and validation sets starts to diminish. This expresses the model's transition towards a certain degree of generalisation, enabling it to adapt to novel, unseen samples to some extent. As the training nears completion, the divergence between the losses of the training and validation sets reaches its minimum, with slight fluctuations occurring thereafter.

In conclusion, considering the analysis of the loss reduction graphs across various methods and the examination of training and

Table 5
Comparison of the training time of one iteration across the seven models.

Models	The training set iteration time in the CJ water area (unit: s)	The training set iteration time in the CP water area (unit: s)
RNN	44.62	46.72
LSTM	52.49	54.69
GRU	46.51	48.74
Bi-LSTM	81.92	90.13
Bi-GRU	69.21	73.31
Seq2Seq	65.48	68.85
Transformer	85.63	87.85

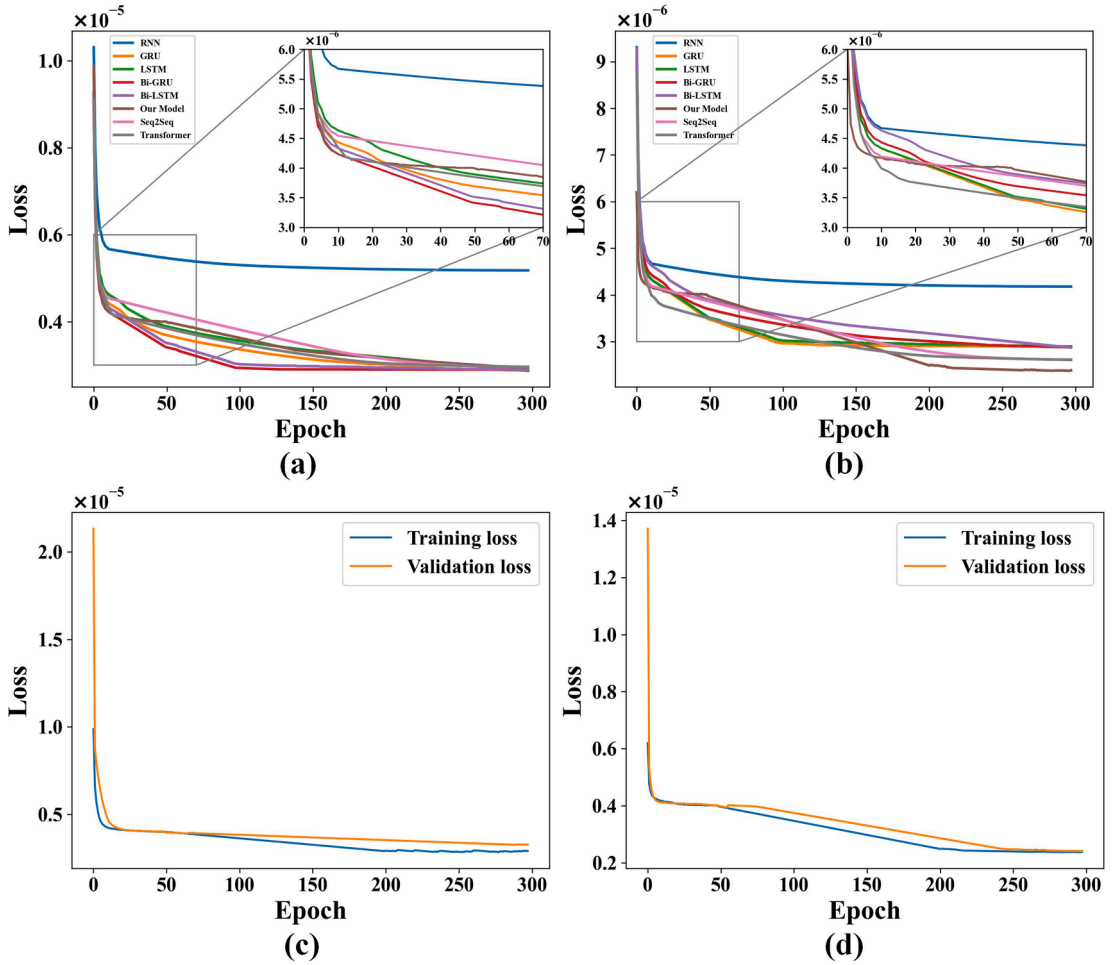

Fig. 15. Visualisation results of loss function descent curve, (a) the result in the CJ water area, (b) the result in the CP water area, (c) train and validation loss in the CJ water area, and (d) train and validation loss in the CP water area.

validation loss, it can be deduced that the proposed DBDIE model exhibits superior performance among the eight prediction methods. It is true for both the training and validation sets, with no substantial indications of overfitting. The trends in loss values consistently hold, and the disparity between the training and validation sets gradually diminishes. The findings suggest that the proposed DBDIE model possesses a reasonable degree of generalisation and is capable of making accurate predictions on previously unseen samples.

5.3. Evaluation indexes

Multiple evaluation indicators are introduced to investigate the prediction accuracy comprehensively from the error rate, similarity, and distance. They calculate the deviation between ground truth and predicted values following the models in Eqs. (21)–(26). More specifically, they are MSE, MAE, MAPE, SMAPE, FD, and AED. y_i is the ith actual value of the ground truth, while $\hat{y}_i$ is the ith predicted value. n indicates overall data points.

MSE reflects the mean value for the square error between the estimated and the actual data, shown in Eq. (21). It can evaluate the degree of variability. It is a statistical measure and loss function commonly used in regression models. The lower its value, the more accurate the prediction model.

$$MSE = \frac{1}{n}\sum_{i=1}^{n}(\hat{y}_i - y_i)^2. \tag{21}$$

MAE measures the error between observed and actual values, the arithmetic mean of the absolute errors, listed in Eq. (22). Since it does not have the issue of errors cancelling each other, the magnitude of the prediction error can be correctly reflected. The prediction model performs better when its value is lower.

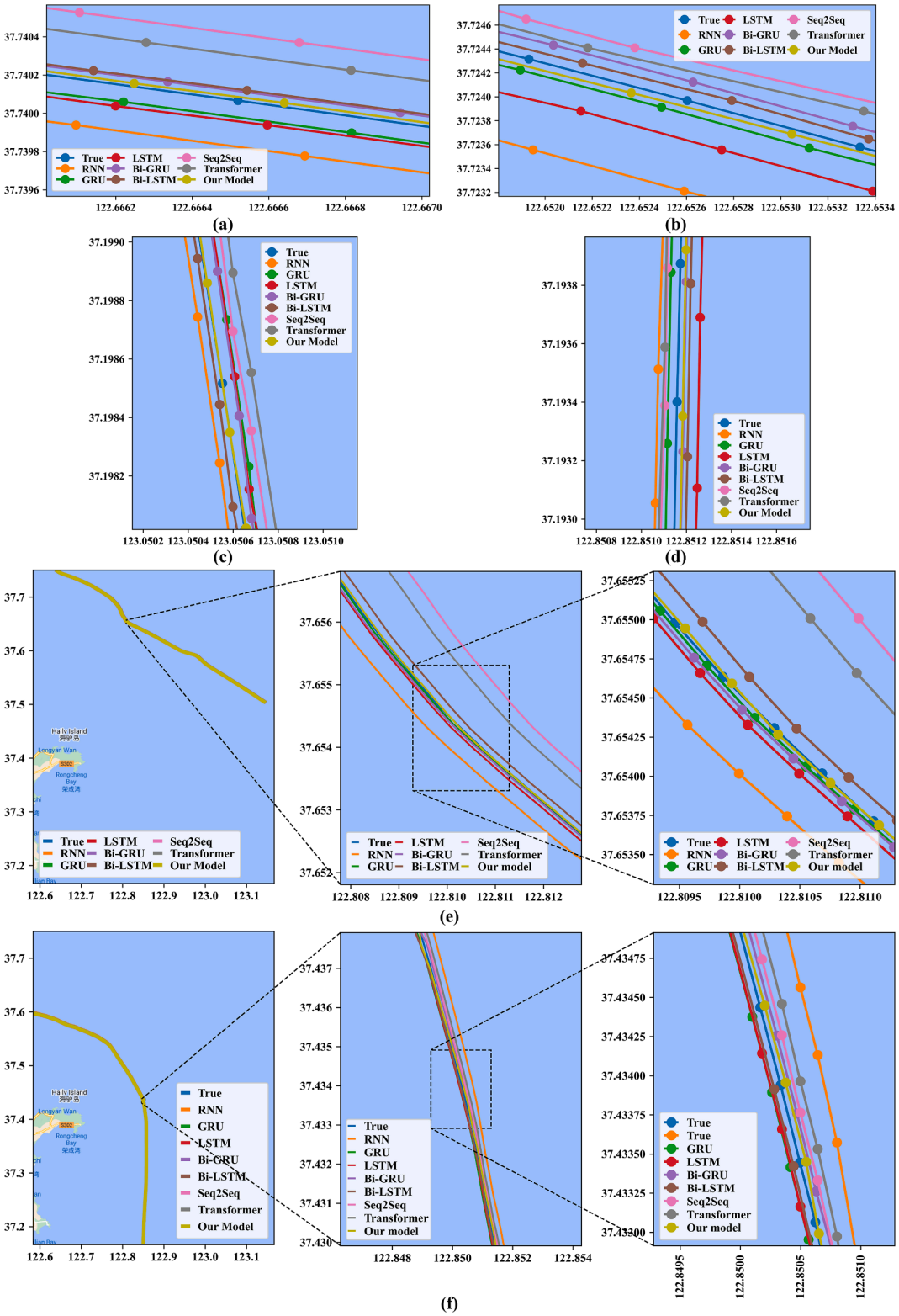

Fig. 16. The comparison of predicted and actual trajectories in the CJ water area.

$$MAE = \frac{1}{n}\sum_{i=1}^{n}|\widehat{y}_i - y_i|. \tag{22}$$

MAPE is the average of the absolute percentage error, shown in Eq. (23). It is commonly used as a statistical measure of prediction accuracy and can describe the accuracy of a series.

$$MAPE = \frac{1}{n}\sum_{i=1}^{n}\left|\frac{\widehat{y}_i - y_i}{y_i}\right| \times 100\%. \tag{23}$$

SMAPE overcomes the asymmetry that occurs with MAPE above, which means the infinity of the prediction is higher than the actual situation listed in Eq. (24).

Table 6
The results for six indices of the tested trajectories in the CJ water area.

	Criteria	RNN	LSTM	GRU	Bi-LSTM	Bi-GRU	Seq2Seq	Transformer	DBDIE Model
1	MSE	4.99E−05	4.98E−08	3.94E−08	3.98E−08	3.79E−08	1.40E−05	6.00E−07	3.09E−08
	MAE	4.25E−03	1.54E−04	1.32E−04	1.25E−04	1.22E−04	2.87E−03	5.93E−04	1.16E−04
	MAPE	6.02E−03	1.94E−04	1.96E−04	1.66E−04	1.54E−04	4.06E−03	8.54E−04	1.45E−04
	SMAPE	6.02E−03	1.94E−04	1.96E−04	1.66E−04	1.54E−04	4.07E−03	8.66E−04	1.45E−04
	FD	3.62E−02	1.48E−03	1.45E−03	1.39E−03	1.24E−03	1.88E−02	3.23E−03	1.17E−03
	AED	6.71E−03	2.55E−04	1.99E−04	1.94E−04	1.97E−04	4.55E−03	8.91E−04	1.91E−04
2	MSE	6.80E−06	3.88E−08	2.85E−08	3.00E−08	2.93E−08	5.00E−06	2.00E−07	2.75E−08
	MAE	1.73E−03	1.31E−04	1.01E−04	1.02E−04	9.92E−05	1.71E−03	3.96E−04	9.86E−05
	MAPE	2.44E−03	1.80E−04	1.49E−04	1.60E−04	1.47E−04	2.60E−03	5.66E−04	1.42E−04
	SMAPE	2.43E−03	1.80E−04	1.49E−04	1.60E−04	1.47E−04	2.61E−03	5.79E−04	1.42E−04
	FD	1.26E−02	1.31E−03	1.27E−03	1.21E−03	1.28E−03	8.90E−03	2.12E−03	1.16E−03
	AED	2.66E−03	2.01E−04	1.48E−04	1.49E−04	1.50E−04	2.60E−03	5.91E−04	1.47E−04
3	MSE	2.82E−05	1.32E−07	1.07E−07	1.04E−07	1.02E−07	1.30E−05	6.00E−07	9.38E−08
	MAE	3.38E−03	2.13E−04	1.55E−04	1.61E−04	1.51E−04	2.62E−03	5.97E−04	1.49E−04
	MAPE	4.52E−03	2.81E−04	2.24E−04	2.47E−04	2.23E−04	3.82E−03	8.06E−04	2.17E−04
	SMAPE	4.54E−03	2.81E−04	2.24E−04	2.47E−04	2.23E−04	3.99E−03	8.16E−04	2.17E−04
	FD	2.63E−02	7.32E−03	7.09E−03	7.30E−03	7.07E−03	1.83E−02	7.00E−03	6.84E−03
	AED	5.36E−03	3.36E−04	2.38E−04	2.44E−04	2.31E−04	4.08E−03	9.22E−04	2.29E−04
4	MSE	3.78E−05	4.98E−08	4.13E−08	3.71E−08	3.55E−08	1.00E−05	5.00E−07	3.24E−08
	MAE	3.59E−03	1.43E−04	1.22E−04	1.08E−04	1.07E−04	2.46E−03	5.09E−04	1.06E−04
	MAPE	4.74E−03	1.70E−04	1.69E−04	1.50E−04	1.41E−04	3.15E−03	6.68E−04	1.37E−04
	SMAPE	4.75E−03	1.70E−04	1.69E−04	1.50E−04	1.41E−04	3.17E−03	6.78E−04	1.37E−04
	FD	3.05E−02	2.23E−03	2.23E−03	2.03E−03	2.00E−03	1.55E−02	3.84E−03	1.97E−03
	AED	5.77E−03	2.40E−04	1.86E−04	1.72E−04	1.69E−04	4.04E−03	7.96E−04	1.56E−04
5	MSE	8.70E−06	7.15E−07	7.12E−07	7.11E−07	7.09E−07	1.30E−05	1.40E−06	6.89E−07
	MAE	1.95E−03	5.00E−04	4.97E−04	5.22E−04	4.95E−04	3.34E−03	8.82E−04	4.98E−04
	MAPE	3.03E−03	7.91E−04	7.87E−04	7.90E−04	7.90E−04	5.51E−03	1.41E−03	7.24E−04
	SMAPE	3.13E−03	7.91E−04	7.87E−04	7.90E−04	7.90E−04	5.54E−03	1.41E−03	7.24E−04
	FD	1.30E−02	7.77E−03	7.69E−03	7.70E−03	7.70E−03	1.22E−02	8.58E−03	7.56E−03
	AED	2.94E−03	7.17E−04	7.15E−04	7.19E−04	7.12E−04	4.78E−03	1.26E−03	7.03E−04
6	MSE	8.11E−05	1.26E−07	1.11E−07	8.83E−08	8.37E−08	7.20E−05	1.00E−06	7.79E−08
	MAE	6.94E−03	2.07E−04	2.06E−04	1.45E−04	1.44E−04	6.55E−03	8.97E−04	1.36E−04
	MAPE	1.19E−02	4.54E−04	3.86E−04	2.98E−04	2.74E−04	1.48E−02	1.62E−03	2.73E−04
	SMAPE	1.16E−02	4.54E−04	3.86E−04	2.98E−04	2.74E−04	1.42E−02	1.62E−03	2.73E−04
	FD	3.69E−02	6.10E−03	6.16E−03	6.06E−03	5.97E−03	2.50E−02	7.38E−03	5.96E−03
	AED	1.04E−02	3.44E−04	3.22E−04	2.37E−04	2.34E−04	1.09E−02	1.38E−03	2.20E−04
7	MSE	6.89E−05	3.02E−07	3.02E−07	2.96E−07	2.84E−07	4.40E−05	1.00E−06	2.83E−07
	MAE	6.42E−03	2.90E−04	2.87E−04	2.79E−04	2.73E−04	5.17E−03	6.80E−04	2.61E−04
	MAPE	1.36E−02	5.98E−04	5.87E−04	5.55E−04	5.41E−04	1.15E−02	1.30E−03	5.33E−04
	SMAPE	1.38E−02	5.98E−04	5.87E−04	5.55E−04	5.44E−04	1.15E−02	1.31E−03	5.33E−04
	FD	2.80E−02	6.86E−03	6.71E−03	6.81E−03	6.57E−03	2.06E−02	8.11E−03	6.49E−03
	AED	9.95E−03	4.47E−04	4.38E−04	4.18E−04	4.16E−04	8.51E−03	1.07E−03	4.02E−04
8	MSE	6.44E−05	1.44E−07	1.41E−07	1.16E−07	1.09E−07	7.60E−05	9.00E−07	1.02E−07
	MAE	6.37E−03	2.33E−04	2.16E−04	1.70E−04	1.65E−04	7.20E−03	8.31E−04	1.64E−04
	MAPE	9.93E−03	4.23E−04	3.99E−04	3.10E−04	2.83E−04	1.44E−02	1.37E−03	2.81E−04
	SMAPE	9.98E−03	4.23E−04	3.99E−04	3.10E−04	2.83E−04	1.45E−02	1.38E−03	2.81E−04
	FD	2.74E−02	3.22E−03	3.15E−03	3.26E−03	3.13E−03	2.07E−02	4.11E−03	2.95E−03
	AED	9.80E−03	3.66E−04	3.52E−04	2.76E−04	2.68E−04	1.10E−02	1.28E−03	2.63E−04
9	MSE	1.21E−04	6.07E−07	5.73E−07	5.94E−07	5.62E−07	7.40E−05	2.00E−06	5.35E−07
	MAE	9.05E−03	4.40E−04	4.58E−04	4.37E−04	4.35E−04	7.34E−03	1.14E−03	4.10E−04
	MAPE	1.59E−02	8.66E−04	8.58E−04	8.59E−04	8.54E−04	1.31E−02	2.13E−03	8.54E−04
	SMAPE	1.59E−02	8.66E−04	8.58E−04	8.59E−04	8.54E−04	1.32E−02	2.14E−03	8.54E−04
	FD	3.89E−02	6.62E−03	6.32E−03	6.47E−03	6.26E−03	2.51E−03	7.03E−03	6.12E−03
	AED	1.33E−02	7.24E−04	7.22E−04	7.18E−04	7.17E−04	1.09E−03	1.76E−03	7.11E−04

$$SMAPE = \frac{1}{n}\sum_{i=1}^{n}\frac{|\widehat{y}_i - y_i|}{(|\widehat{y}_i| + |y_i|)/2} \times 100\%. \tag{24}$$

FD is a curve similarity metric that considers both the position and arrangement of curve points, as shown in Eq. (25).

$$FD = \max\left(\sqrt{\sum_{i=1}^{n}(\widehat{y}_i - y_i)^2}\right). \tag{25}$$

AED is a commonly adopted definition of distance and means the precise distance between two places in space, listed in Eq. (26). It is the average Euclidean distance.

$$AED = \frac{1}{n}\sqrt{\sum_{i=1}^{n}(\widehat{y}_i - y_i)^2}. \tag{26}$$

The six indices above provide a holistic view of prediction accuracy from various perspectives. MAE calculates the absolute errors between actual and predicted data, while the average squared errors between them can be represented using MSE. MAPE and SMAPE can quantify the accuracy in terms of percentage. FD describes the similarity of the path space. AED calculates the mean distance between two spatial trajectories.

5.4. Comparative analysis in the CJ water area

5.4.1. Visual analysis of prediction results

For a detailed comparative analysis of the prediction performance among the eight models, nine representative trajectories from the CJ water area in the test set are chosen. Fig. 16 displays four representative trajectories, where the prediction results obtained from the eight models are highlighted using distinct colours. In Fig. 16 (a)–(d), the blue line indicates the actual trajectory (i.e. the ground

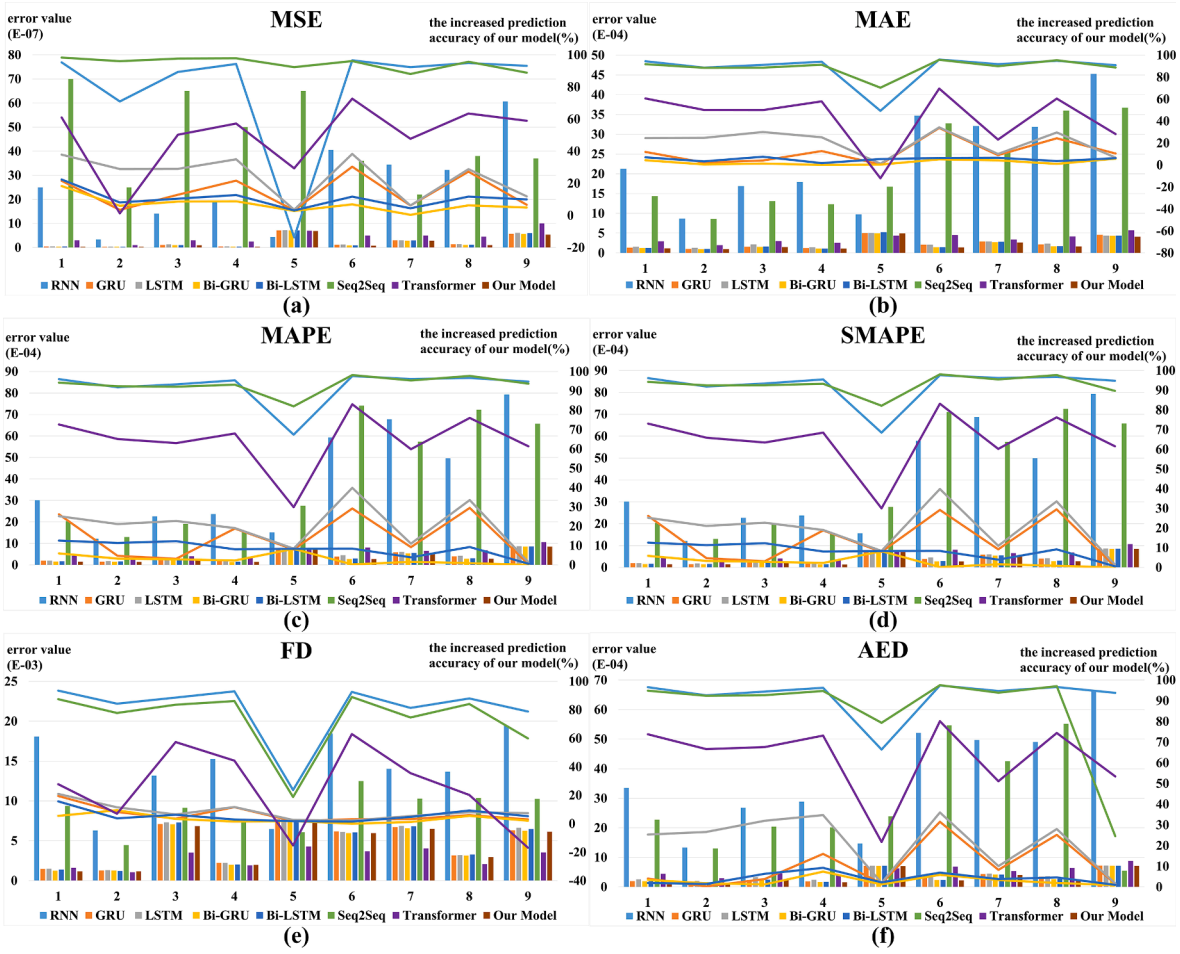

Fig. 17. The experimental six-index error histogram and accuracy improvement line graphs in the CJ water area.

truth). The lines of other colours represent the predicted trajectories of the eight models. The dots denote specific latitude and longitude points. Fig. 16 (a)–(b) and Fig. 16 (c)–(d) compare trajectories in different directions, while Fig. 16 (e) and Fig. 16 (f) show the differences in trajectories from the global to local part.

In summary, the trajectory predicted by the DBDIE model exhibits the closest resemblance to the actual trajectory, verifying the DBDIE model as the most accurate predictor among the eight tested models. The prediction accuracy of RNN and Seq2Seq is the lowest. There was little difference in accuracy between the bi-directional models.

5.4.2. Quantitative evaluation of different methods

Nine trajectories with different features in the test set are used for comparing the performance of prediction models. Their MMSIs are numbered 1–9, corresponding to 241407000, 241408000, 249020000, 353816000, 412362000, 412536000, 412550870, 412551020, and 413115000, respectively. The nine selected trajectories are compared with the ground truth based on the eight prediction models. The evaluation results of eight models are listed in Table 6, and the minimum errors are highlighted in bold. The comprehensive comparison results prove that the performance of the new DBDIE model is the best among the eight models in six kinds of evaluation methods, providing effective evidence supporting the viability of the proposed DBDIE model.

Furthermore, a more accurate comparison of the performance of the eight models is conducted from a data perspective. The newly introduced DBDIE model exhibits the least error across the six metrics for the tested trajectories, resulting in its delivery of more accurate prediction results. The performance of the bi-directional networks is also good but worse than the new DBDIE model.

The error histograms for each model against the six indices in the CJ water area and the line graphs of accuracy improvement of the new model compared with the other seven models are shown in Fig. 17 (a)–(f). The histogram is a statistical representation of the data in Table 5. The improvement percentages in accuracy against six evaluation indexes can be calculated using the ratio of the error difference between the new DBDIE and the other models.

It can be seen from Fig. 17 that the improvement range of the six indexes is stable between 0 and 100 %. The average improvement percentages of six evaluation indexes can be obtained by statistics on the data of four comparisons, shown in Table 7.

According to the average improvement percentages of six evaluation indexes, the proposed DBDIE model has the top two largest improvements when compared with RNN and Seq2Seq, followed by Transformer, LSTM, GRU, Bi-LSTM, and Bi-GRU.

For the MSE index, the comparison results of the DBDIE model and the other seven models following the order in Table 7 are 79.30 %, 24.42 %, 14.82 %, 10.51 %, 7.03 %, 97.69 % and 49.14 %, respectively. For the MAE index, the accuracy of the new DBDIE model has the biggest improvement of 88.94 % and the lowest improvement of 2.56 % compared with other models. For the MAPE and SMAPE indexes, the average improvement percentages of the comparisons are very close, with the highest of about 93.24 % and the lowest of about 2.82 %. For the FD index, the values remain between 3.42 % and 80.46 %. For the AED index, the proposed DBDIE model improves by 85.22 % compared to Seq2Seq and 3.02 % compared to Bi-GRU. Therefore, the results of six evaluation indexes (i.e. the improved accuracy) verify that the newly proposed DBDIE model is superior to the other seven prediction models.

5.5. Comparative analysis in the CP water area

5.5.1. Visual analysis of prediction results

The nine typical trajectories in the CP water area are selected for testing and visualisation. Similar to the experimental process in Section 5.4.1, the comparative results are obtained in the CP water area. The visualisation results of four representative trajectories are shown in Fig. 18 (a)–(f). The superiority of the proposed DBDIE model becomes evident as its predicted trajectory exhibits the closest match to the actual trajectory (ground truth) in comparison to the results obtained from the other seven models.

5.5.2. Quantitative evaluation of different methods

Nine trajectories with different features in the CP water area are selected to compare the performance of prediction models. Their MMSIs are numbered 1–9, corresponding to 209047000, 259739000, 355356000, 373498000, 518100230, 538006066, 566410000, 636091132, and 636092704, respectively. Similar to the experimental process in Section 5.4.2, the evaluation results of eight models are listed in Table 7. The proposed DBDIE model has the smallest prediction error values for the nine tested trajectories among eight models, shown in bold in Table 8.

In the CP water area, the proposed DBDIE model has the lowest prediction error, which indicates its prediction performance is the best of the eight models. From the comparison results in Tables 6 and 8, the magnitudes of error for the same index in these two water areas are basically similar to each other, demonstrating the applicability of the proposed model to deal with massive data in different

Table 7
The average improvement percentages of the six indices in the CJ water area.

Index	MSE	MAE	MAPE	SMAPE	FD	AED
DBDIE vs RNN	79.30 %	87.94 %	92.19 %	92.31 %	80.46 %	92.09 %
DBDIE vs LSTM	24.42 %	20.74 %	20.27 %	20.27 %	8.53 %	21.83 %
DBDIE vs GRU	14.82 %	12.13 %	14.36 %	14.35 %	6.70 %	10.25 %
DBDIE vs Bi-LSTM	10.51 %	5.29 %	8.32 %	8.32 %	5.72 %	4.17 %
DBDIE vs Bi-GRU	7.03 %	2.56 %	2.82 %	2.82 %	3.42 %	3.02 %
DBDIE vs Seq2Seq	97.69 %	88.96 %	93.24 %	92.83 %	73.53 %	85.22 %
DBDIE vs Transformer	49.12 %	43.12 %	64.33 %	64.67 %	24.79 %	62.45 %

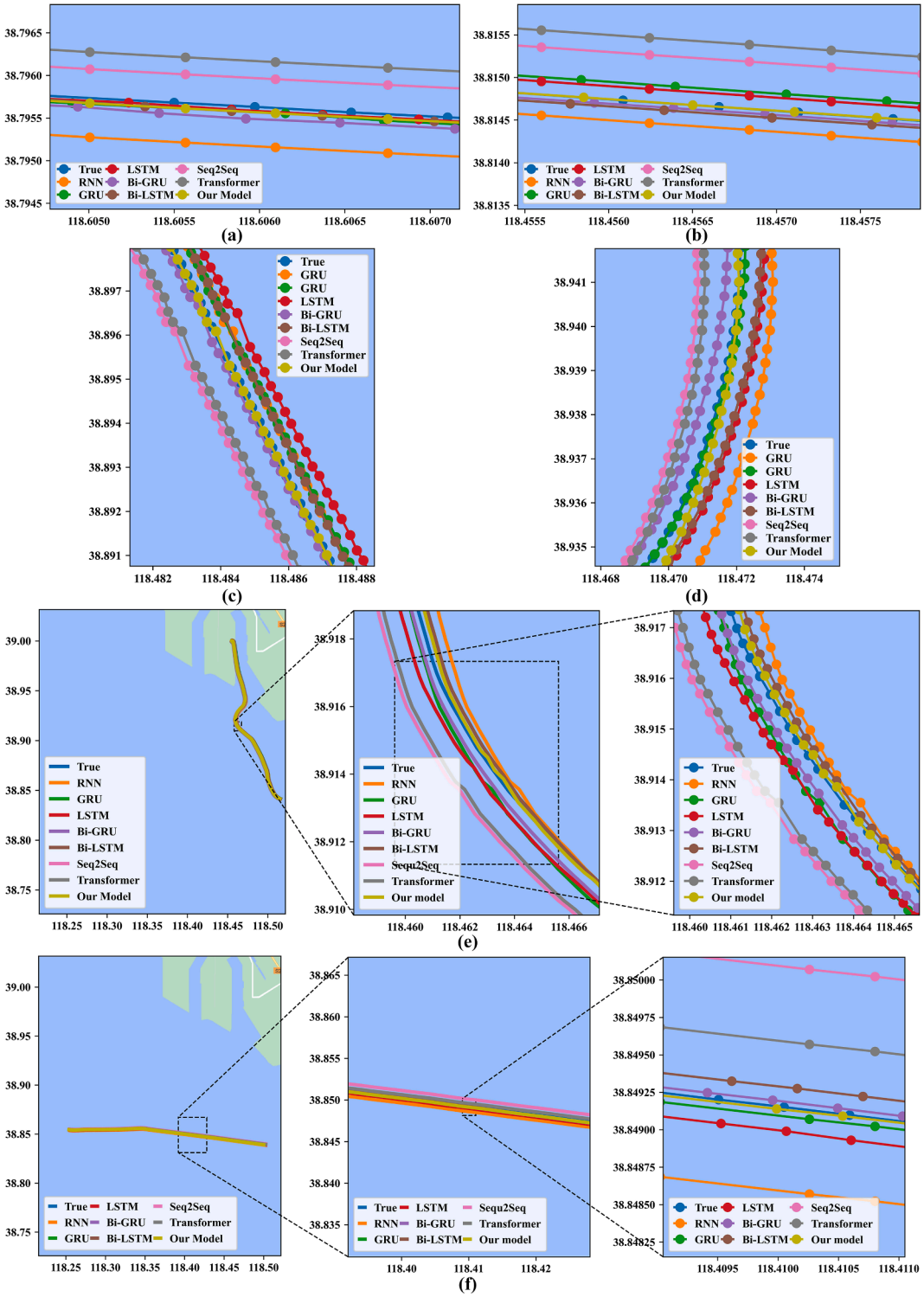

Fig. 18. The comparison of predicted and actual trajectories in the CP water area.

water areas. The error histograms and the line graphs of accuracy improvement are also implemented in the CP water area, shown in Fig. 19.

Similar to the analytical process in Section 5.4.2, the average improvement percentages of six indexes can be obtained by statistics on the data of seven comparisons, shown in Table 9. The improvement percentages of the six indexes are between 10 % and 60 %, with

Table 8
The results for six indices of nine test trajectories in the CP water area.

	Criteria	RNN	LSTM	GRU	Bi-LSTM	Bi-GRU	Seq2Seq	Transformer	DBDIE Model
1	MSE	2.11E−04	4.48E−07	4.48E−07	6.76E−07	3.35E−07	6.32E−04	8.00E−07	1.47E−07
	MAE	8.94E−03	3.85E−04	3.85E−04	5.64E−04	3.81E−04	1.11E−02	5.30E−04	2.68E−04
	MAPE	9.58E−03	3.65E−04	3.65E−04	5.39E−04	3.77E−04	1.15E−02	5.42E−04	2.98E−04
	SMAPE	9.59E−03	3.65E−04	3.65E−04	5.39E−04	3.77E−04	1.16E−02	5.55E−04	2.98E−04
	FD	5.09E−02	2.47E−03	2.47E−03	2.36E−03	1.86E−03	1.09E−01	6.66E−03	1.59E−03
	AED	1.57E−02	7.33E−04	7.33E−04	1.06E−03	7.06E−04	1.98E−02	9.59E−04	4.73E−04
2	MSE	1.99E−04	5.46E−07	5.46E−07	4.65E−07	4.83E−07	2.17E−04	2.30E−06	2.48E−07
	MAE	9.35E−03	4.39E−04	4.39E−04	4.16E−04	4.36E−04	5.95E−03	9.16E−04	2.91E−04
	MAPE	9.38E−03	4.24E−04	4.24E−04	4.07E−04	4.55E−04	6.55E−03	9.27E−04	3.32E−04
	SMAPE	9.40E−03	4.24E−04	4.24E−04	4.07E−04	4.55E−04	6.59E−03	9.46E−04	3.32E−04
	FD	5.14E−02	1.22E−02	1.22E−02	1.20E−02	1.21E−02	1.05E−01	7.91E−03	1.17E−02
	AED	1.71E−02	8.27E−04	8.27E−04	7.79E−04	7.91E−04	1.03E−02	1.67E−03	5.17E−04
3	MSE	6.09E−05	7.05E−07	7.05E−07	5.35E−07	3.36E−07	8.40E−05	1.10E−06	2.69E−07
	MAE	5.87E−03	4.50E−04	4.50E−04	4.50E−04	2.89E−04	4.78E−03	7.42E−04	2.49E−04
	MAPE	7.46E−03	4.19E−04	4.19E−04	4.14E−04	2.76E−04	6.48E−03	9.76E−04	2.51E−04
	SMAPE	7.49E−03	4.19E−04	4.19E−04	4.14E−04	2.76E−04	6.50E−03	9.99E−04	2.51E−04
	FD	2.67E−02	1.35E−02	1.35E−02	1.30E−02	1.28E−02	5.74E−02	5.13E−03	1.17E−02
	AED	9.43E−03	8.60E−04	8.60E−04	8.63E−04	5.45E−04	7.36E−03	1.16E−03	4.61E−04
4	MSE	6.00E−07	2.80E−07	2.80E−07	2.79E−07	2.79E−07	4.00E−06	3.00E−07	2.79E−07
	MAE	2.80E−04	4.70E−04	4.70E−04	4.92E−04	6.74E−04	1.33E−03	1.30E−04	4.06E−04
	MAPE	4.00E−04	5.81E−04	5.81E−04	7.22E−04	8.10E−04	1.26E−03	2.45E−04	5.38E−04
	SMAPE	4.00E−04	5.81E−04	5.81E−04	7.22E−04	8.10E−04	1.28E−03	2.62E−04	5.37E−04
	FD	1.57E−02	3.66E−02	3.66E−02	3.66E−02	3.66E−02	2.32E−02	1.86E−02	3.65E−02
	AED	4.29E−04	7.77E−04	7.77E−04	8.25E−04	1.12E−03	2.58E−03	2.06E−04	6.51E−04
5	MSE	4.11E−05	6.31E−07	6.31E−07	2.86E−07	3.16E−07	1.60E−05	3.00E−07	2.53E−07
	MAE	5.69E−03	3.98E−04	3.98E−04	4.45E−04	4.03E−04	3.40E−03	3.41E−04	3.24E−04
	MAPE	7.90E−03	4.41E−04	4.41E−04	5.65E−04	5.05E−04	4.50E−03	4.43E−04	4.38E−04
	SMAPE	7.90E−03	4.41E−04	4.41E−04	5.65E−04	5.05E−04	4.53E−03	4.45E−04	4.38E−04
	FD	1.06E−02	5.39E−03	5.39E−03	3.15E−03	3.21E−03	1.79E−02	5.99E−03	2.154–03
	AED	8.72E−03	7.08E−04	7.08E−04	7.27E−04	6.66E−04	5.41E−03	5.79E−04	5.53E−04
6	MSE	2.98E−05	5.92E−07	5.92E−07	4.85E−07	5.47E−07	4.80E−05	1.67E−05	4.21E−07
	MAE	4.24E−03	4.26E−04	4.26E−04	3.92E−04	3.96E−04	4.33E−03	1.81E−03	3.25E−04
	MAPE	5.63E−03	4.25E−04	4.25E−04	3.91E−04	4.17E−04	5.57E−03	2.30E−03	3.60E−04
	SMAPE	5.65E−03	4.25E−04	4.25E−04	3.91E−04	4.17E−04	5.56E−03	2.29E−03	3.60E−04
	FD	2.16E−02	2.31E−02	2.31E−02	2.30E−02	2.30E−02	3.01E−02	2.57E−02	2.27E−02
	AED	6.72E−03	7.96E−04	7.96E−04	7.32E−04	7.21E−04	7.17E−03	3.04E−03	5.84E−04
7	MSE	9.53E−05	5.62E−07	5.62E−07	4.69E−07	5.32E−07	3.38E−04	1.60E−06	2.34E−07
	MAE	6.65E−03	4.40E−04	4.40E−04	4.24E−04	4.56E−04	1.11E−02	8.92E−04	2.66E−04
	MAPE	7.45E−03	4.21E−04	4.21E−04	4.15E−04	4.73E−04	1.28E−02	9.44E−04	3.14E−04
	SMAPE	7.46E−03	4.21E−04	4.21E−04	4.15E−04	4.73E−04	1.28E−02	9.85E−04	3.14E−04
	FD	2.36E−02	1.51E−02	1.51E−02	1.50E−02	1.50E−02	4.99E−02	7.29E−03	1.47E−02
	AED	1.14E−02	8.34E−04	8.34E−04	7.93E−04	8.35E−04	1.86E−02	1.58E−03	4.71E−04
8	MSE	1.79E−05	1.01E−06	1.01E−06	9.88E−07	8.05E−07	4.00E−06	2.00E−07	7.38E−07
	MAE	3.58E−03	4.52E−04	4.52E−04	4.39E−04	2.67E−04	1.71E−03	3.34E−04	2.53E−04
	MAPE	4.76E−03	4.84E−04	4.82E−04	4.58E−04	3.13E−04	2.80E−03	4.65E−04	2.79E−04
	SMAPE	4.78E−03	4.82E−04	4.82E−04	4.58E−04	3.12E−04	2.79E−03	4.77E−04	2.79E−04
	FD	8.45E−03	3.56E−02	3.56E−02	3.54E−02	3.54E−02	7.05E−03	4.58E−03	3.51E−02
	AED	5.64E−03	8.26E−04	8.26E−04	8.15E−04	4.77E−04	2.67E−03	5.32E−04	4.67E−04
9	MSE	9.33E−05	5.39E−07	5.39E−07	8.82E−07	3.15E−07	1.98E−05	4.00E−07	1.23E−07
	MAE	6.55E−03	4.44E−04	4.44E−04	6.48E−04	3.65E−04	2.91E−03	4.88E−04	2.37E−04
	MAPE	6.71E−03	4.09E−04	4.09E−04	5.83E−04	3.42E−04	3.18E−03	5.80E−04	2.50E−04
	SMAPE	6.73E−03	4.09E−04	4.09E−04	5.83E−04	3.42E−04	3.19E−03	5.50E−04	2.50E−04
	FD	3.81E−02	2.74E−03	2.74E−03	3.24E−03	3.08E−03	1.98E−02	2.85E−03	1.88E−03
	AED	1.18E−02	8.55E−04	8.55E−04	1.25E−03	6.92E−04	5.08E−03	8.28E−04	4.27E−04

the highest of 52.195 % and the lowest of 11.345 %. Compared with the CJ water area, the improvement in the CP water area is more significant. Therefore, the results of six indices and the improved accuracy in the CP water area further verify that the new DBDIE model outperforms the other seven models.

5.6. Ablation experiments

This section primarily focuses on comparing the performance of different variants of the proposed DBDIE by ablation experiments. Various attention mechanism methods are employed while keeping the two bidirectional network units consistent to demonstrate the effectiveness of each method. The descriptions of different attention mechanism methods (i.e. A1–A4) are as follows:

(1) A1: Linear projection-based attention mechanism method.

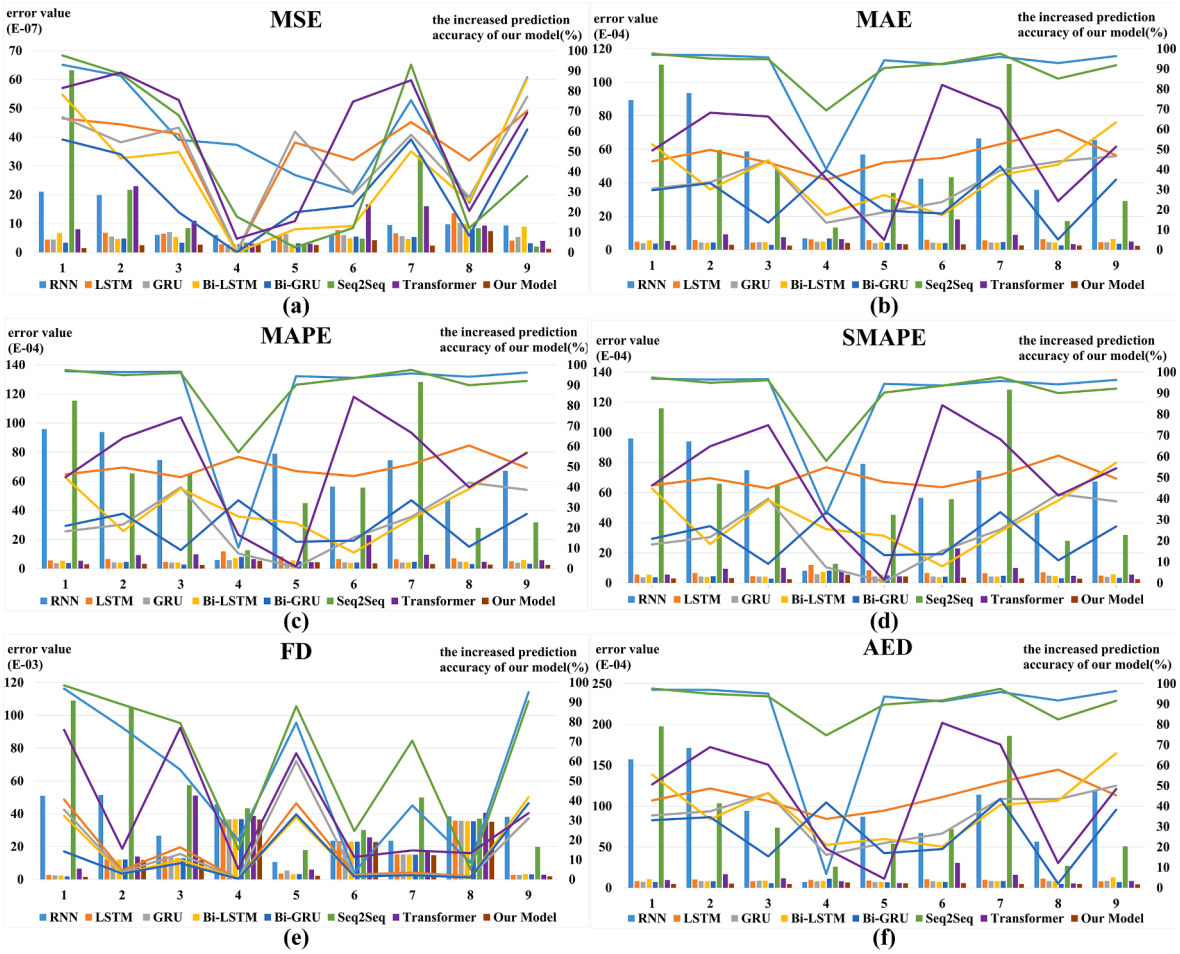

Fig. 19. The experimental six-index error histogram and accuracy improvement line graphs in the CP water area.

Table 9
The average improvement percentages in the CP water area.

Index	MSE	MAE	MAPE	SMAPE	FD	AED
DBDIE vs RNN	60.47 %	89.08 %	86.05 %	88.55 %	52.68 %	84.97 %
DBDIE vs LSTM	52.19 %	46.70 %	50.01 %	50.01 %	15.42 %	44.99 %
DBDIE vs GRU	48.37 %	32.74 %	23.28 %	23.29 %	16.62 %	35.66 %
DBDIE vs Bi-LSTM	40.08 %	36.85 %	30.97 %	30.97 %	13.74 %	38.87 %
DBDIE vs Bi-GRU	32.54 %	26.14 %	20.96 %	20.96 %	11.34 %	27.20 %
DBDIE vs Seq2Seq	47.72 %	90.47 %	89.88 %	89.98 %	62.31 %	90.46 %
DBDIE vs Transformer	60.12 %	50.20 %	49.82 %	51.65 %	34.57 %	46.10 %

Initially, the input undergoes encoding through Bi-GRU and Bi-LSTM to generate their respective outputs. Subsequently, a Multi-Layer Perceptron (MLP) is applied to each model's output for dimensionality reduction and nonlinear transformation, resulting in two sub-feature vectors. These vectors are concatenated, and finally, attention weights are computed using two separate linear projection layers.

(2) A2: Soft attention mechanism-based method.

First, the input is encoded using Bi-GRU and Bi-LSTM, leading to corresponding outputs. Then, the outputs are subject to dimensionality reduction and non-linearly transformation using an MLP, yielding four sub-feature vectors. Each sub-feature vector is then processed by a projection layer composed of two linear layers with a nonlinear activation function to calculate attention weights. Finally, the attention weights are obtained by mapping the sub-feature vectors to a higher-dimensional space and applying a softmax function.

(3) A3: Using a method that combines multiple sub-attention mechanisms.

The attention mechanisms mentioned above are individually applied to the outputs of both Bi-GRU and Bi-LSTM units, generating their respective outputs. Subsequently, an MLP is employed for each model's output to perform dimensionality reduction and nonlinear transformation, producing two sub-feature vectors. These vectors are concatenated, and attention weights are calculated using two separate linear projection layers.

(4) A4: Using the DBDIE model proposed in this article.

The input is encoded using Bi-GRU and Bi-LSTM to obtain corresponding outputs. Subsequently, these outputs are subjected to dimensionality reduction and nonlinear transformation using an MLP, resulting in four sub-feature vectors. These vectors are stacked to form a new tensor. The features within this tensor are then processed through a projection layer consisting of two linear layers with a nonlinear activation function. Finally, the resulting tensor is normalized using a softmax function, yielding attention weights.

Tables 10 and 11 represent the results of ablation experiments by employing four attention mechanism methods on fusing Bi-GRU and Bi-LSTM units, respectively. In these experiments, the nine selected test trajectories from the previously mentioned comparative experiments are individually utilised for two water areas.

By comparing the detailed data provided above, the improvement percentage of the proposed DBDIE model for each attention mechanism method can be calculated, as presented in Tables 12 and 13. In both water areas, the attention mechanisms designed by the proposed DBDIE model achieved significantly better results than the other three cases (i.e. A1–A3). Specifically, in the CJ water region, the proposed DBDIE model shows an average enhancement of 47.33 %, and in the CP water region, an improvement of 72.93 %.

Tables 12 and 13 demonstrate the average percentage improvement of the ablation experiments in the CJ and CP water areas, respectively. In both tables, it's evident that the DBDIE model surpasses A1, A2, and A3 across various metrics, verifying varied degrees of improvement. Therefore, the effectiveness of the proposed DBDIE model has been further verified.

5.7. Discussion

The bar and line charts in Fig. 20 depict the average improvement percentages in prediction accuracy of the DBDIE method across six evaluation metrics when contrasted with the other seven models. It is apparent that the results of the proposed DBDIE model have been improved compared to the other seven models by the results from the two different water areas in Fig. 20. Meantime, the trends of the six indexes in the two water areas are consistent at large, which can, in turn, verify the effectiveness of the proposed DBDIE model. In two different test sets, the most significant improvement can be seen by the comparison with LSTM. The overall accuracy improvement is consistently centred between 2 % and 98 %.

The average accuracy improvement percentages in terms of six indices in the two water areas are presented in Table 14. It is evident that the new DBDIE model has improved prediction accuracy. Specifically, the average improvement percentages can be as high as 88.58 % and 78.47 % in the CJ and CP water areas, respectively. Compared with the other seven models, Bi-LSTM and Bi-GRU usually have better prediction results than LSTM and GRU. Therefore, their improvement percentages are relatively lower than those of LSTM and GRU. The average improvement percentages in terms of the six indicators in the two water areas further demonstrate the prediction effectiveness and high applicability of the proposed DBDIE model.

5.8. Implications

The findings of this research can provide value to various stakeholders in the shipping industry, including MASS manufacturers, operators, and authorities. How each of these groups might benefit is shown below.

(1) Manufacturers of MASS could use the new ship trajectory prediction model to enhance the autonomy and safety of their vessels. By predicting the future trajectory of a ship, an autonomous vessel could adjust its course or speed to avoid collisions, optimise its route, or respond to changing environmental conditions. This could improve the efficiency and reliability of shipping operations, reduce the risk of accidents, and potentially lower the costs associated with operating MASS.
(2) Shipping operators could benefit from ship trajectory prediction results by using them to optimise their fleet management, reduce costs, and enhance safety. By analysing the predicted trajectories of ships in their fleet, operators could identify potential congestion or collision risks and adjust their operations accordingly. They could also use trajectory prediction to optimise route planning, fuel consumption, and vessel speeds, resulting in cost savings and reduced emissions.
(3) Maritime authorities, such as port operators or maritime traffic controllers, could use ship trajectory prediction results to enhance their situational awareness and improve the safety of shipping traffic. Authorities can better manage traffic flow, allocate resources more efficiently, and detect potential collision hazards by forecasting ships' future trajectories within their territories. This could result in improved safety, reduced congestion, and more efficient use of port infrastructure.

Overall, ship trajectory prediction possesses the potential to benefit extensive stakeholders in the shipping industry by improving safety, reducing costs, and enhancing efficiency.

Table 10
The results of the ablation experiments in the CJ water area.

	Criteria	A1	A2	A3	A4 (DBDIE)
1	MSE	1.55E−07	1.09E−07	1.20E−07	3.10E−08
	MAE	2.35E−04	1.85E−04	2.05E−04	1.17E−04
	MAPE	3.04E−04	2.56E−04	2.86E−04	1.45E−04
	SMAPE	3.04E−04	2.56E−04	2.86E−04	1.45E−04
	FD	7.06E−03	6.64E−03	7.05E−03	1.17E−03
	AED	3.85E−04	2.92E−04	3.18E−04	1.91E−04
2	MSE	6.23E−07	5.28E−07	5.89E−07	2.76E−08
	MAE	6.00E−04	4.72E−04	4.76E−04	9.87E−05
	MAPE	1.07E−03	9.28E−04	9.12E−04	1.43E−04
	SMAPE	1.07E−03	9.28E−04	9.12E−04	1.43E−04
	FD	5.68E−03	6.00E−03	6.32E−03	1.17E−03
	AED	9.22E−04	7.61E−04	7.61E−04	1.48E−04
3	MSE	1.17E−07	9.94E−08	9.90E−08	9.39E−08
	MAE	2.59E−04	1.56E−04	1.50E−04	1.49E−04
	MAPE	2.87E−04	2.60E−04	2.70E−04	2.17E−04
	SMAPE	2.87E−04	2.60E−04	2.70E−04	2.17E−04
	FD	7.69E−03	7.08E−03	7.00E−03	6.84E−03
	AED	4.52E−04	2.39E−04	2.37E−04	2.29E−04
4	MSE	6.83E−07	6.89E−07	6.77E−07	3.24E−08
	MAE	5.36E−04	5.25E−04	5.08E−04	1.07E−04
	MAPE	8.44E−04	8.36E−04	8.12E−04	1.38E−04
	SMAPE	8.44E−04	8.36E−04	8.12E−04	1.38E−04
	FD	7.42E−03	7.47E−03	7.60E−03	1.97E−03
	AED	7.80E−04	7.59E−04	7.29E−04	1.57E−04
5	MSE	7.53E−07	7.96E−07	7.59E−07	6.90E−07
	MAE	5.02E−04	5.53E−04	5.50E−04	4.98E−04
	MAPE	8.34E−04	8.46E−04	8.04E−04	7.25E−04
	SMAPE	8.34E−04	8.46E−04	8.04E−04	7.25E−04
	FD	8.19E−03	8.33E−03	8.48E−03	7.56E−03
	AED	8.27E−04	8.35E−04	8.35E−04	7.04E−04
6	MSE	8.80E−08	8.08E−08	8.85E−08	7.80E−08
	MAE	1.45E−04	1.43E−04	1.48E−04	1.37E−04
	MAPE	2.89E−04	2.87E−04	2.83E−04	2.73E−04
	SMAPE	2.89E−04	2.87E−04	2.83E−04	2.73E−04
	FD	6.36E−03	6.13E−03	6.06E−03	5.97E−03
	AED	2.97E−04	2.77E−04	2.76E−04	2.21E−04
7	MSE	3.00E−07	9.69E−07	8.99E−07	2.84E−07
	MAE	3.59E−04	3.85E−04	3.91E−04	2.61E−04
	MAPE	6.26E−04	6.69E−04	6.46E−04	5.33E−04
	SMAPE	6.26E−04	6.69E−04	6.46E−04	5.33E−04
	FD	6.65E−03	6.98E−03	6.95E−03	6.49E−03
	AED	5.32E−04	4.10E−04	4.10E−04	4.03E−04
8	MSE	3.33E−07	2.73E−07	2.98E−07	1.03E−07
	MAE	4.25E−04	3.17E−04	3.10E−04	1.64E−04
	MAPE	8.34E−04	6.54E−04	6.19E−04	2.81E−04
	SMAPE	8.34E−04	6.54E−04	6.19E−04	2.81E−04
	FD	6.51E−03	6.38E−03	6.64E−03	2.96E−03
	AED	6.31E−04	4.92E−04	4.67E−04	2.64E−04
9	MSE	5.60E−07	5.61E−07	5.41E−07	5.35E−07
	MAE	4.39E−04	4.31E−04	4.39E−04	4.11E−04
	MAPE	8.77E−04	8.62E−04	8.63E−04	8.54E−04
	SMAPE	8.77E−04	8.62E−04	8.63E−04	8.54E−04
	FD	6.31E−03	6.30E−03	6.32E−03	6.13E−03
	AED	7.52E−04	7.32E−04	7.30E−04	7.12E−04

6. Conclusion

Ship trajectory prediction can provide important information to practitioners in various maritime activities. It plays a vital role in detecting abnormal ship behaviours and collision warnings. This paper introduces a novel DBDIE prediction model that integrates two bi-directional networks and optimises the weights of model units based on an attention mechanism. High-quality AIS data from two typical water areas are used for experimental tests to test and ensure the validity of the results. Furthermore, the paper conducts a comparative analysis with other prediction models, including RNN, LSTM, GRU, Bi-LSTM, Bi-GRU, Seq2Seq, and Transformer, both in theory and experiments. Six different indexes are employed to measure the outcomes of all models. Additionally, ablation experiments are performed to further verify the effectiveness of the proposed DBDIE model. The results demonstrate that the newly proposed DBDIE model outperforms the other models in ship trajectory prediction, solidifying its superior performance and potential practical applicability. This research helps manned ships to realise the prediction with high accuracy and MASS to make more reasonable

Table 11
The results of the ablation experiments in the CP water area.

	Criteria	A1	A2	A3	A4 (DBDIE)
1	MSE	2.85E−07	1.89E−07	2.58E−07	1.48E−07
	MAE	5.13E−04	4.89E−04	3.26E−04	2.68E−04
	MAPE	3.48E−04	3.20E−04	3.73E−04	2.98E−04
	SMAPE	3.48E−04	3.20E−04	3.73E−04	2.98E−04
	FD	1.96E−03	1.79E−03	1.79E−03	1.60E−03
	AED	6.85E−04	6.43E−04	6.92E−04	4.73E−04
2	MSE	3.62E−06	2.59E−06	2.38E−06	2.48E−07
	MAE	4.24E−04	3.93E−04	3.90E−04	2.92E−04
	MAPE	7.40E−04	5.53E−04	5.30E−04	3.33E−04
	SMAPE	7.40E−04	5.53E−04	5.30E−04	3.33E−04
	FD	4.97E−02	4.68E−02	4.51E−02	1.17E−02
	AED	6.38E−04	6.61E−04	6.47E−04	5.18E−04
3	MSE	8.98E−07	5.82E−07	3.58E−07	2.69E−07
	MAE	3.65E−04	3.87E−04	3.35E−04	2.50E−04
	MAPE	4.94E−04	4.25E−04	2.68E−04	2.52E−04
	SMAPE	4.94E−04	4.25E−04	2.68E−04	2.52E−04
	FD	1.85E−02	1.79E−02	1.92E−02	1.18E−02
	AED	5.96E−04	5.15E−04	5.12E−04	4.61E−04
4	MSE	3.92E−06	2.97E−06	2.56E−06	2.80E−07
	MAE	5.94E−04	4.15E−04	4.78E−04	4.07E−04
	MAPE	7.20E−04	6.15E−04	5.48E−04	5.38E−04
	SMAPE	7.20E−04	6.15E−04	5.48E−04	5.38E−04
	FD	8.49E−02	8.01E−02	7.84E−02	3.66E−02
	AED	7.10E−04	7.04E−04	6.94E−04	6.52E−04
5	MSE	5.76E−07	2.59E−07	3.96E−07	2.53E−07
	MAE	4.17E−04	4.32E−04	4.07E−04	3.24E−04
	MAPE	4.52E−04	4.75E−04	4.97E−04	4.39E−04
	SMAPE	4.52E−04	4.75E−04	4.97E−04	4.39E−04
	FD	7.37E−03	6.27E−03	7.89E−03	2.15E−03
	AED	5.55E−04	5.99E−04	6.64E−04	5.53E−04
6	MSE	3.90E−06	2.75E−06	2.54E−06	4.22E−07
	MAE	4.29E−04	3.87E−04	3.82E−04	3.25E−04
	MAPE	7.44E−04	5.17E−04	5.09E−04	3.61E−04
	SMAPE	7.44E−04	5.17E−04	5.09E−04	3.61E−04
	FD	6.76E−02	6.55E−02	6.77E−02	2.27E−02
	AED	6.44E−04	6.46E−04	6.32E−04	5.85E−04
7	MSE	4.84E−06	3.68E−06	3.40E−06	2.34E−07
	MAE	4.60E−04	3.51E−04	3.34E−04	2.67E−04
	MAPE	8.16E−04	6.87E−04	6.51E−04	3.14E−04
	SMAPE	8.16E−04	6.87E−04	6.51E−04	3.14E−04
	FD	5.19E−02	4.92E−02	4.62E−02	1.47E−02
	AED	7.08E−04	5.68E−04	5.39E−04	4.71E−04
8	MSE	9.73E−07	9.04E−07	8.67E−07	7.39E−07
	MAE	2.78E−04	3.44E−04	3.03E−04	2.53E−04
	MAPE	4.48E−04	3.51E−04	2.95E−04	2.79E−04
	SMAPE	4.48E−04	3.51E−04	2.95E−04	2.79E−04
	FD	3.63E−02	9.63E−02	8.17E−02	3.51E−02
	AED	5.09E−04	5.19E−04	6.63E−04	4.67E−04
9	MSE	1.00E−06	3.40E−07	2.05E−07	1.23E−07
	MAE	2.86E−04	2.46E−04	2.92E−04	2.38E−04
	MAPE	4.67E−04	2.62E−04	3.83E−04	2.51E−04
	SMAPE	4.67E−04	2.62E−04	3.83E−04	2.51E−04
	FD	2.56E−03	3.26E−03	2.36E−03	1.89E−03
	AED	5.17E−04	6.24E−04	5.78E−04	4.28E−04

Table 12
The average percentage increase of the ablation experiments in the CJ water area.

	MSE	MAE	MAPE	SMAPE	FD	AED
Compared with A1	43.26 %	39.75 %	38.80 %	38.80 %	35.65 %	43.58 %
Compared with A2	46.88 %	33.30 %	36.12 %	36.12 %	35.01 %	31.75 %
Compared with A3	47.33 %	33.99 %	35.81 %	35.81 %	35.41 %	31.76 %

operation strategies and improve the efficiency and safety of marine traffic.

Although some effective results have been achieved, the current model only examines the latitude and longitude information of the historical trajectories. Ship navigation is a complex and changing process. Therefore, it is still a challenge to make reliable analyses and

Table 13
The average percentage increase of the ablation experiments in the CP water area.

	MSE	MAE	MAPE	SMAPE	FD	AED
Compared with A1	72.93 %	28.50 %	38.17 %	38.17 %	47.33 %	16.54 %
Compared with A2	57.69 %	22.58 %	24.06 %	24.06 %	53.38 %	15.74 %
Compared with A3	57.07 %	19.27 %	21.97 %	21.97 %	51.16 %	17.76 %

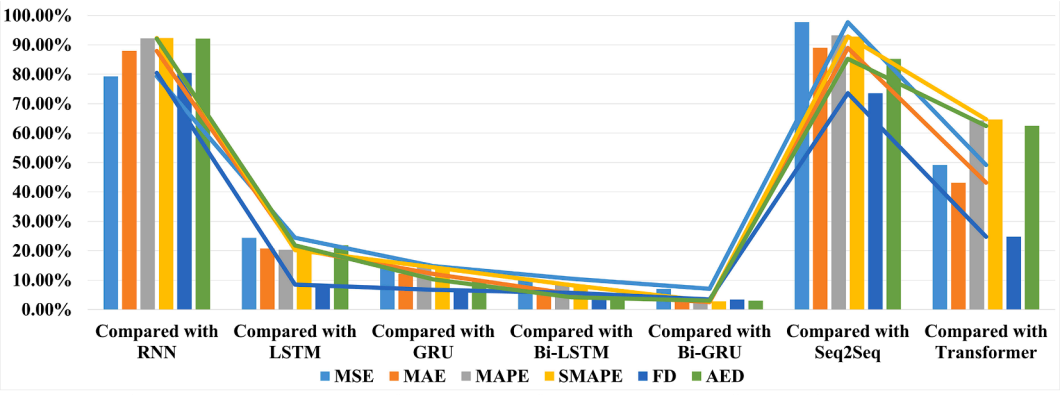

(a) The average percentage improvement in model accuracy for the CJ water area

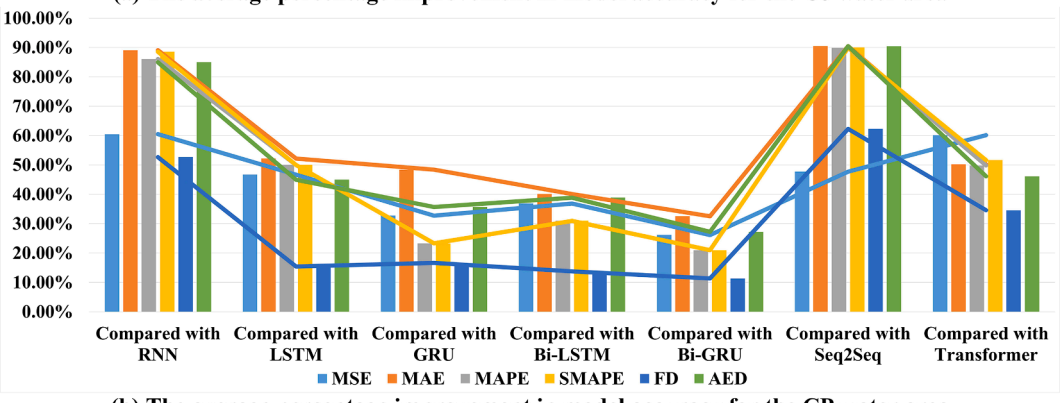

(b) The average percentage improvement in model accuracy for the CP water area

Fig. 20. The average improvement percentages of the proposed DBDIE model in two water areas.

Table 14
The average improvement percentages in the six indexes compared with the other seven models.

Water areas	RNN	LSTM	GRU	Bi-LSTM	Bi-GRU	Seq2Seq	Transformer
CJ	87.37 %	19.34 %	12.10 %	7.05 %	3.61 %	88.58 %	51.41 %
CP	76.97 %	43.22 %	29.99 %	31.91 %	23.19 %	78.47 %	48.75 %

predictions by considering multiple factors (e.g. COG and SOG) based on the available data. In the future, various ways of model fusion can be further explored to improve prediction accuracy.

CRediT authorship contribution statement

Huanhuan Li: Conceptualization, Methodology, Validation, Formal analysis, Investigation, Resources, Project administration, Data curation, Software, Supervision, Visualization, Writing – original draft, Writing – review & editing. **Wenbin Xing:** Validation, Formal analysis, Investigation, Software, Visualization, Writing – original draft, Writing – review & editing. **Hang Jiao:** Validation, Formal analysis, Writing – review & editing. **Zaili Yang:** Validation, Resources, Writing – review & editing, Project administration, Funding acquisition. **Yan Li:** Formal analysis, Validation, Visualization.

Declaration of competing interest

The authors declare the following financial interests/personal relationships which may be considered as potential competing interests: Zaili Yang reports financial support was provided by European Research Council.

Data availability

Data will be made available on request.

Acknowledgements

This work is supported by the European Research Council project (TRUST CoG 2019 864724) and Royal Society International Exchanges 2021 Cost Share (NSFC) (IEC\NSFC\211211).

References

Alessandrini, A., Mazzarella, F., Vespe, M., 2019. Estimated time of arrival using historical vessel tracking data. IEEE Trans. Intell. Transp. Syst. 20, 7–15. https://doi.org/10.1109/TITS.2017.2789279.
Alizadeh, D., Alesheikh, A.A., Sharif, M., 2021. Vessel trajectory prediction using historical automatic identification system data. J. Navig. 74, 156–174. https://doi.org/10.1017/S0373463320000442.
Bai, X., Hou, Y., Yang, D., 2021. Choose clean energy or green technology? Empirical evidence from global ships. Transp. Res. Part E: Logist. Transp. Rev. 151, 102364 https://doi.org/10.1016/j.tre.2021.102364.
Bao, K., Bi, J., Gao, M., Sun, Y., Zhang, X., Zhang, W., 2022. An improved ship trajectory prediction based on AIS data using MHA-BiGRU. J. Mar. Sci. Eng. 10, 804 https://doi.org/10.3390/jmse10060804.
Chang, C.-H., Kontovas, C., Yu, Q., Yang, Z., 2021. Risk assessment of the operations of maritime autonomous surface ships. Reliab. Eng. Syst. Saf. 207, 107324 https://doi.org/10.1016/j.ress.2020.107324.
Chen, C.M., 2006. CiteSpace II: detecting and visualizing emerging trends and transient patterns in scientific literature. J. Am. Soc. Inf. Sci. Technol. 57, 359–377. https://doi.org/10.1002/asi.20317.
Chen, L., Hopman, H., Negenborn, R.R., 2018. Distributed model predictive control for vessel train formations of cooperative multi-vessel systems. Transp. Res. Part C: Emerg. Technol. 92, 101–118. https://doi.org/10.1016/j.trc.2018.04.013.
Chen, Y., Yang, S., Suo, Y., Zheng, M., 2021. Ship track prediction based on DLGWO-SVR. Sci. Program. 2021, 9085617 https://doi.org/10.1155/2021/9085617.
Coraddu, A., Oneto, L., de Maya, B.N., Kurt, R., 2020. Determining the most influential human factors in maritime accidents: a data-driven approach. Ocean Eng. 211, 107588 https://doi.org/10.1016/j.oceaneng.2020.107588.
Filom, S., Amiri, A.M., Razavi, S., 2022. Applications of machine learning methods in port operations – a systematic literature review. Transp. Res. Part E: Logist. Transp. Rev. 161, 102722 https://doi.org/10.1016/j.tre.2022.102722.
Fratila, G., Nita, S.C., Hrebenciuc, A., 2021. The importance of maritime transport for economic growth in the European Union: a panel data analysis. Sustainability 13, 7961. https://doi.org/10.3390/su13147961.
Gao, R., Li, R., Hu, M., Suganthan, P.N., Yuen, K.F., 2023a. Dynamic ensemble deep echo state network for significant wave height forecasting. Appl. Energy 329, 120261. https://doi.org/10.1016/j.apenergy.2022.120261.
Gao, R., Li, R., Hu, M., Suganthan, P.N., Yuen, K.F., 2023b. Online dynamic ensemble deep random vector functional link neural network for forecasting. Neural Netw. 166, 51–69. https://doi.org/10.1016/j.neunet.2023.06.042.
Goerlandt, F., 2020. Maritime Autonomous Surface Ships from a risk governance perspective: interpretation and implications. Saf. Sci. 128, 104758 https://doi.org/10.1016/j.ssci.2020.104758.
Harati-Mokhtari, A., Wall, A., Brooks, P., Wang, J., 2007. Automatic identification system (AIS): data reliability and human error implications. J. Navig. 60, 373–389. https://doi.org/10.1017/S0373463307004298.
Huang, P., Chen, Q., Wang, D., Wang, M., Wu, X., Huang, X., 2022. TripleConvTransformer: a deep learning vessel trajectory prediction method fusing discretized meteorological data. Front. Environ. Sci. 10, 1012547 https://doi.org/10.3389/fenvs.2022.1012547.
Kim, K.-I., Lee, K.M., 2018. Deep learning-based caution area traffic prediction with automatic identification system sensor data. Sensors 18, 3172. https://doi.org/10.3390/s18093172.
Kisialiou, Y., Gribkovskaia, I., Laporte, G., 2018. Robust supply vessel routing and scheduling. Transp. Res. Pt. C-Emerg. Technol. 90, 366–378. https://doi.org/10.1016/j.trc.2018.03.012.
LeCun, Y., Bengio, Y., Hinton, G., 2015. Deep learning. Nature 521, 436–444. https://doi.org/10.1038/nature14539.
Lei, P.-R., 2016. A framework for anomaly detection in maritime trajectory behavior. Knowl. Inf. Syst. 47, 189–214. https://doi.org/10.1007/s10115-015-0845-4.
Li, Y., Bai, X., Wang, Q., Ma, Z., 2022b. A big data approach to cargo type prediction and its implications for oil trade estimation. Transp. Res. Part E: Logist. Transp. Rev. 165, 102831 https://doi.org/10.1016/j.tre.2022.102831.
Li, Y., Liang, M., Li, H., Yang, Z., Du, L., Chen, Z., 2023. Deep learning-powered vessel traffic flow prediction with spatial-temporal attributes and similarity grouping. Eng. Appl. Artif. Intell. 126, 107012. https://doi.org/10.1016/j.engappai.2023.107012.
Li, H., Liu, J., Liu, R.W., Xiong, N., Wu, K., Kim, T.H., 2017. A dimensionality reduction-based multi-step clustering method for robust vessel trajectory analysis. Sensors 17 (8), 1792. https://doi.org/10.3390/s17081792.
Li, H., Liu, J., Wu, K., Yang, Z., Liu, R.W., Xiong, N., 2018. Spatio-temporal vessel trajectory clustering based on data mapping and density. IEEE Access 6, 58939–58954. https://doi.org/10.1109/ACCESS.2018.2866364.
Li, H., Liu, J., Yang, Z., Liu, R.W., Wu, K., Wan, Y., 2020. Adaptively constrained dynamic time warping for time series classification and clustering. Inf. Sci. 534, 97–116. https://doi.org/10.1016/j.ins.2020.04.009.
Li, H., Jiao, H., Yang, Z., 2023. Ship trajectory prediction based on machine learning and deep learning: A systematic review and methods analysis. Eng. Appl. Artif. Intell. 126, 107062. https://doi.org/10.1016/j.engappai.2023.107062.
Li, H., Lam, J.S.L., Yang, Z., Liu, J., Liu, R.W., Liang, M., Li, Y., 2022a. Unsupervised hierarchical methodology of maritime traffic pattern extraction for knowledge discovery. Transp. Res. Part C: Emerg. Technol. 143, 103856 https://doi.org/10.1016/j.trc.2022.103856.
Li, H., Jiao, H., Yang, Z., 2023a. AIS data-driven ship trajectory prediction modelling and analysis based on machine learning and deep learning methods. Transp. Res. Part E: Logist. Transp. Rev. 175, 103152 https://doi.org/10.1016/j.tre.2023.103152.
Li, H., Ren, X., Yang, Z., 2023b. Data-driven Bayesian network for risk analysis of global maritime accidents. Reliab. Eng. Syst. Saf. 230, 108938.
Li, H., Yang, Z., 2023. Incorporation of AIS data-based machine learning into unsupervised route planning for maritime autonomous surface ships. Transp. Res. Part E: Logist. Transp. Rev. 176, 103171 https://doi.org/10.1016/j.tre.2023.103171.
Liang, M., Liu, R.W., Zhan, Y., Li, H., Zhu, F., Wang, F.-Y., 2022. Fine-grained vessel traffic flow prediction with a spatio-temporal multigraph convolutional network. IEEE Trans. Intell. Transp. Syst. 23, 23694–23707. https://doi.org/10.1109/TITS.2022.3199160.

Liu, C., Guo, S., Feng, Y., Hong, F., Huang, H., Guo, Z., 2019a. L-VTP: long-term vessel trajectory prediction based on multi-source data analysis. Sensors 19, 4365. https://doi.org/10.3390/s19204365.
Liu, C., Chu, X., Wu, W., Li, S., He, Z., Zheng, M., Zhou, H., Li, Z., 2022. Human-machine cooperation research for navigation of maritime autonomous surface ships: a review and consideration. Ocean Eng. 246, 110555 https://doi.org/10.1016/j.oceaneng.2022.110555.
Liu, J., Shi, G., Zhu, K., 2019b. Vessel trajectory prediction model based on AIS sensor data and adaptive chaos differential evolution support vector regression (ACDE-SVR). Appl. Sci.-Basel 9, 2983. https://doi.org/10.3390/app9152983.
Luo, M., Shin, S.-H., 2019. Half-century research developments in maritime accidents: future directions. Accid. Anal. Prev. 123, 448–460. https://doi.org/10.1016/j.aap.2016.04.010.
Ma, J., Jia, C., Yang, X., Cheng, X., Li, W., Zhang, C., 2020. A data-driven approach for collision risk early warning in vessel encounter situations using attention-BiLSTM. IEEE Access 8, 188771–188783. https://doi.org/10.1109/ACCESS.2020.3031722.
Ma, J., Jia, C., Shu, Y., Liu, K., Zhang, Y., Hu, Y., 2021. Intent prediction of vessels in intersection waterway based on learning vessel motion patterns with early observations. Ocean Eng. 232, 109154 https://doi.org/10.1016/j.oceaneng.2021.109154.
Ma, H., Zuo, Y., Li, T., 2022. Vessel navigation behavior analysis and multiple-trajectory prediction model based on AIS Data. J. Adv. Transp. 2022, 6622862 https://doi.org/10.1155/2022/6622862.
Martin-Martin, A., Orduna-Malea, E., Thelwall, M., Delgado Lopez-Cozar, E., 2018. Google Scholar, Web of Science, and Scopus: a systematic comparison of citations in 252 subject categories. J. Informetr. 12, 1160–1177. https://doi.org/10.1016/j.joi.2018.09.002.
Maskooki, A., Virjonen, P., Kallio, M., 2021. Assessing the prediction uncertainty in a route optimization model for autonomous maritime logistics. Int. Trans. Oper. Res. 28, 1765–1786. https://doi.org/10.1111/itor.12882.
Mehri, S., Alesheikh, A.A., Basiri, A., 2021. A contextual hybrid model for vessel movement prediction. IEEE Access 9, 45600–45613. https://doi.org/10.1109/ACCESS.2021.3066463.
Murray, B., Perera, L.P., 2020. A dual linear autoencoder approach for vessel trajectory prediction using historical AIS data. Ocean Eng. 209, 107478 https://doi.org/10.1016/j.oceaneng.2020.107478.
Pallotta, G., Vespe, M., Bryan, K., 2013. Vessel pattern knowledge discovery from AIS data: a framework for anomaly detection and route prediction. Entropy 15, 2218–2245. https://doi.org/10.3390/e15062218.
Park, J., Jeong, J., Park, Y., 2021. Ship trajectory prediction based on Bi-LSTM using spectral-clustered AIS data. J. Mar. Sci. Eng. 9, 1037 https://doi.org/10.3390/jmse9091037.
Perera, L.P., Oliveira, P., Soares, C.G., 2012. Maritime traffic monitoring based on vessel detection, tracking, state estimation, and trajectory prediction. IEEE Trans. Intell. Transp. Syst. 13, 1188–1200. https://doi.org/10.1109/TITS.2012.2187282.
Qian, L., Zheng, Y., Li, L., Ma, Y., Zhou, C., Zhang, D., 2022. A New method of inland water ship trajectory prediction based on long short-term memory network optimized by genetic algorithm. Appl. Sci.-Basel 12, 4073. https://doi.org/10.3390/app12084073.
Ramos, M.A., Utne, I.B., Mosleh, A., 2019. Collision avoidance on maritime autonomous surface ships: operators' tasks and human failure events. Saf. Sci. 116, 33–44. https://doi.org/10.1016/j.ssci.2019.02.038.
Rong, H., Teixeira, A.P., Guedes Soares, C., 2019. Ship trajectory uncertainty prediction based on a Gaussian Process model. Ocean Eng. 182, 499–511. https://doi.org/10.1016/j.oceaneng.2019.04.024.
Rong, H., Teixeira, A.P., Guedes Soares, C., 2022. Maritime traffic probabilistic prediction based on ship motion pattern extraction. Reliab. Eng. Syst. Saf. 217, 108061 https://doi.org/10.1016/j.ress.2021.108061.
Sanchez-Gonzalez, P.-L., Diaz-Gutierrez, D., Leo, T.J., Nunez-Rivas, L.R., 2019. Toward digitalization of maritime transport? Sensors 19, 926. https://doi.org/10.3390/s19040926.
Scheepens, R., van de Wetering, H., van Wijk, J.J., 2014. Contour based visualization of vessel movement predictions. Int. J. Geogr. Inf. Sci. 28, 891–909. https://doi.org/10.1080/13658816.2013.868466.
Schmidhuber, J., 2015. Deep learning in neural networks: an overview. Neural Netw. 61, 85–117. https://doi.org/10.1016/j.neunet.2014.09.003.
Sorensen, K.A., Heiselberg, P., Heiselberg, H., 2022. Probabilistic maritime trajectory prediction in complex scenarios using deep learning. Sensors 22, 2058. https://doi.org/10.3390/s22052058.
Statheros, T., Howells, G., McDonald-Maier, K., 2008. Autonomous ship collision avoidance navigation concepts, technologies and techniques. J. Navig. 61, 129–142. https://doi.org/10.1017/S037346330700447X.
Suo, Y., Chen, W., Claramunt, C., Yang, S., 2020. A ship trajectory prediction framework based on a recurrent neural network. Sensors 20, 5133. https://doi.org/10.3390/s20185133.
Sutulo, S., Moreira, L., Soares, C.G., 2002. Mathematical models for ship path prediction in manoeuvring simulation systems. Ocean Eng. 29, 1–19. https://doi.org/10.1016/S0029-8018(01)00023-3.
Synnestvedt, M.B., Chen, C., Holmes, J.H., 2005. CiteSpace II: visualization and knowledge discovery in bibliographic databases. AMIA Annu. Symp. Proc. 2005, 724–728.
Tang, H., Wei, L., Yin, Y., Shen, H., Qi, Y., 2020. Detection of abnormal vessel behaviour based on probabilistic directed graph model. J. Navig. 73, 1014–1035. https://doi.org/10.1017/S0373463320000144.
Tu, E., Zhang, G., Rachmawati, L., Rajabally, E., Huang, G.-B., 2018. Exploiting AIS data for intelligent maritime navigation: a comprehensive survey from data to methodology. IEEE Trans. Intell. Transp. Syst. 19, 1559–1582. https://doi.org/10.1109/TITS.2017.2724551.
Veitch, E., Alsos, O.A., 2022. A systematic review of human-AI interaction in autonomous ship system. Saf. Sci. 152, 105778 https://doi.org/10.1016/j.ssci.2022.105778.
Venskus, J., Treigys, P., Markeviciute, J., 2021. Unsupervised marine vessel trajectory prediction using LSTM network and wild bootstrapping techniques. Nonlinear Anal.-Model Control 26, 718–737. https://doi.org/10.15388/namc.2021.26.23056.
Volkova, T.A., Balykina, Y.E., Bespalov, A., 2021. Predicting ship trajectory based on neural networks using AIS data. J. Mar. Sci. Eng. 9, 254 https://doi.org/10.3390/jmse9030254.
Wang, J., Guo, Y., Wang, Y., 2022. A sequential random forest for short-term vessel speed prediction. Ocean Eng. 248, 110691 https://doi.org/10.1016/j.oceaneng.2022.110691.
Wang, S., He, Z., 2021. A prediction model of vessel trajectory based on generative adversarial network. J. Navig. 74, 1161–1171. https://doi.org/10.1017/S0373463321000382.
Wang, L., Wu, Q., Liu, J., Li, S., Negenborn, R.R., 2019. State-of-the-art research on motion control of maritime autonomous surface ships. J. Mar. Sci. Eng. 7, 438 https://doi.org/10.3390/jmse7120438.
Xiao, Z., Fu, X., Zhang, L., Goh, R.S.M., 2020. Traffic pattern mining and forecasting technologies in maritime traffic service networks: a comprehensive survey. IEEE Trans. Intell. Transp. Syst. 21, 1796–1825. https://doi.org/10.1109/TITS.2019.2908191.
Xiao, Z., Fu, X., Zhao, L., Zhang, L., Teo, T.K., Li, N., Zhang, W., Qin, Z., 2022. Next-generation vessel traffic services systems-from "Passive" to "Proactive". IEEE Intell. Transp. Syst. Mag. 2–16. https://doi.org/10.1109/MITS.2022.3144411.
Xin, X., Liu, K., Loughney, S., Wang, J., Li, H., Yang, Z., 2023a. Graph-based ship traffic partitioning for intelligent maritime surveillance in complex port waters. Expert Syst. Appl. 231, 120825 https://doi.org/10.1016/j.eswa.2023.120825.
Xin, X., Yang, Z., Liu, K., Zhang, J., Wu, X., 2023b. Multi-stage and multi-topology analysis of ship traffic complexity for probabilistic collision detection. Expert Syst. Appl. 213, 118890 https://doi.org/10.1016/j.eswa.2022.118890.
Xing, W., Wang, J., Zhou, K., Li, H., Li, Y., Yang, Z., 2023. A hierarchical methodology for vessel traffic flow prediction using Bayesian tensor decomposition and similarity grouping. Ocean Eng. 286, 115687. https://doi.org/10.1016/j.oceaneng.2023.115687.
Xu, Y., Zhang, J., Ren, Y., Zeng, Y., Yuan, J., Liu, Z., Wang, L., Ou, D., 2022. Improved vessel trajectory prediction model based on stacked-BiGRUs. Secur. Commun. Netw. 2022, 8696558 https://doi.org/10.1155/2022/8696558.

Yan, Y., Chow, A.H.F., Ho, C.P., Kuo, Y.-H., Wu, Q., Ying, C., 2022. Reinforcement learning for logistics and supply chain management: methodologies, state of the art, and future opportunities. Transp. Res. Part E: Logist. Transp. Rev. 162, 102712 https://doi.org/10.1016/j.tre.2022.102712.

Yang, C.-H., Lin, G.-C., Wu, C.-H., Liu, Y.-H., Wang, Y.-C., Chen, K.-C., 2022. Deep learning for vessel trajectory prediction using clustered AIS data. Mathematics 10, 2936. https://doi.org/10.3390/math10162936.

Yang, D., Wu, L., Wang, S., Jia, H., Li, K.X., 2019. How big data enriches maritime research – a critical review of Automatic Identification System (AIS) data applications. Transp. Rev. 39, 755–773. https://doi.org/10.1080/01441647.2019.1649315.

Yang, D., Wu, L., Wang, S., 2021. Can we trust the AIS destination port information for bulk ships?–Implications for shipping policy and practice. Transp. Res. Part E: Logist. Transp. Rev. 149, 102308 https://doi.org/10.1016/j.tre.2021.102308.

Yin, Z., Yang, D., Bai, X., 2022. Vessel destination prediction: a stacking approach. Transp. Res. Pt. C-Emerg. Technol. 145, 103951 https://doi.org/10.1016/j.trc.2022.103951.

You, L., Xiao, S., Peng, Q., Claramunt, C., Han, X., Guan, Z., Zhang, J., 2020. ST-Seq2Seq: a spatio-temporal feature-optimized Seq2Seq model for short-term vessel trajectory prediction. IEEE Access 8, 218565–218574. https://doi.org/10.1109/ACCESS.2020.3041762.

Zhang, C., Bin, J., Wang, W., Peng, X., Wang, R., Halldearn, R., Liu, Z., 2020. AIS data driven general vessel destination prediction: a random forest based approach. Transp. Res. Pt. C-Emerg. Technol. 118, 102729 https://doi.org/10.1016/j.trc.2020.102729.

Zhang, X., Fu, X., Xiao, Z., Xu, H., Qin, Z., 2022. Vessel trajectory prediction in maritime transportation: current approaches and beyond. IEEE Trans. Intell. Transp. Syst. 23, 19980–19998. https://doi.org/10.1109/TITS.2022.3192574.

Zhang, M., Kujala, P., Musharraf, M., Zhang, J., Hirdaris, S., 2023. A machine learning method for the prediction of ship motion trajectories in real operational conditions. Ocean Eng. 283, 114905. https://doi.org/10.1016/j.oceaneng.2023.114905.

Zhang, S., Shi, G., Liu, Z., Zhao, Z., Wu, Z., 2018. Data-driven based automatic maritime routing from massive AIS trajectories in the face of disparity. Ocean Eng. 155, 240–250. https://doi.org/10.1016/j.oceaneng.2018.02.060.

Zhang, L., Zhang, J., Niu, J., Wu, Q.M.J., Li, G., 2021. Track prediction for HF radar vessels submerged in strong clutter based on MSCNN fusion with GRU-AM and AR model. Remote Sens. 13, 2164 https://doi.org/10.3390/rs13112164.

Zhou, Y., Daamen, W., Vellinga, T., Hoogendoorn, S., 2019. Review of maritime traffic models from vessel behavior modeling perspective. Transp. Res. Part C: Emerg. Technol. 105, 323–345. https://doi.org/10.1016/j.trc.2019.06.004.